

# A phylogenetically-restricted essential cell cycle progression factor in the human pathogen *Candida albicans*

**Priya Jaitly**

Jawaharlal Nehru Centre for Advanced Scientific Research

**Melanie Legrand**

Institut Pasteur

**Abhijit Das**

Jawaharlal Nehru Centre for Advanced Scientific Research <https://orcid.org/0000-0002-4891-5037>

**Tejas Patel**

Jawaharlal Nehru Centre for Advanced Scientific Research <https://orcid.org/0000-0002-4623-3657>

**Murielle Chauvel**

Institut Pasteur

**Christophe d'Enfert**

Institut Pasteur <https://orcid.org/0000-0002-6235-3886>

**Kaustuv Sanyal** (✉ [sanyal@jncasr.ac.in](mailto:sanyal@jncasr.ac.in))

Jawaharlal Nehru Centre for Advanced Scientific Research <https://orcid.org/0000-0002-6611-4073>

---

## Article

**Keywords:** *C. albicans*, chromosomal stability, CSA6

**Posted Date:** October 26th, 2021

**DOI:** <https://doi.org/10.21203/rs.3.rs-966555/v1>

**License:** © ⓘ This work is licensed under a Creative Commons Attribution 4.0 International License.

[Read Full License](#)

---

**Version of Record:** A version of this preprint was published at Nature Communications on July 23rd, 2022. See the published version at <https://doi.org/10.1038/s41467-022-31980-3>.

1 **A phylogenetically-restricted essential cell cycle progression factor in the**  
2 **human pathogen *Candida albicans***

3  
4  
5 Priya Jaitly<sup>1</sup>, Mélanie Legrand<sup>2</sup>, Abhijit Das<sup>1†</sup>, Tejas Patel<sup>1†</sup>, Murielle Chauvel<sup>2</sup>, Christophe  
6 d'Enfert<sup>2\*</sup> and Kaustuv Sanyal<sup>1,3\*</sup>

7  
8  
9 <sup>1</sup>Molecular Mycology Laboratory, Molecular Biology and Genetics Unit, Jawaharlal Nehru  
10 Centre for Advanced Scientific Research, Bangalore, India.

11 <sup>2</sup> Institut Pasteur, Université de Paris, INRAE, USC2019, Unité Biologie et Pathogénicité  
12 Fongiques, F-75015 Paris, France.

13 <sup>3</sup>Osaka University, Suita, Osaka, Japan.

14  
15  
16 \* Corresponding authors. Email: christophe.denfert@pasteur.fr, sanyal@jncasr.ac.in

17 † These authors contributed equally to this work.  
18  
19  
20  
21  
22  
23  
24  
25  
26  
27  
28  
29  
30  
31  
32

33 **Abstract**

34

35 Chromosomal instability in fungal pathogens caused by cell division errors is associated with  
36 antifungal drug resistance. To identify mechanisms underlying such instability and to uncover  
37 new potential antifungal targets, we conducted an overexpression screen monitoring chromosomal  
38 stability in the human fungal pathogen *Candida albicans*. Analysis of ~1000 genes uncovered six  
39 chromosomal stability (*CSA*) genes, five of which are related to cell division genes in other  
40 organisms. The sixth gene, *CSA6*, is selectively present in the CUG-Ser clade species that  
41 includes *C. albicans* and other human fungal pathogens. The protein encoded by *CSA6* localizes  
42 to the spindle pole bodies, is required for exit from mitosis, and induces a checkpoint-dependent  
43 metaphase arrest upon overexpression. Together, *Csa6* defines an essential CUG-Ser fungal  
44 clade-specific cell cycle progression factor, highlighting the existence of phylogenetically-  
45 restricted cell division genes which may serve as potential unique therapeutic targets.

46

47 **Teaser**

48

49 *Csa6* is essential for mitotic progression and mitotic exit in the human fungal pathogen *Candida*  
50 *albicans*.

51

52

53

54

55

56

57

58

59

60

61

62

63

64

65

66

## 67 **Introduction**

68

69 Cell division is a fundamental aspect of all living organisms, required to support growth,  
70 reproduction and replenishment of dead or damaged cells. The primary objective of cell division  
71 is to ensure genome stability by preserving and transferring the genetic material with high-fidelity  
72 into progeny. Genome stability is achieved by proper execution of key cell cycle events such as  
73 chromosome duplication at the S phase followed by equal segregation of the duplicated  
74 chromosomes at the M phase. In addition, various cell cycle checkpoints monitor the integrity and  
75 fidelity of cell cycle events in response to an error or any damage until rectified or repaired.  
76 Failure of any of the error-correcting mechanisms can introduce genetic alterations, causing  
77 genomic instability in progeny. Genome instability can occur as a consequence of either point  
78 mutations, insertions or deletions of bases in specific genes and/or gain, loss or rearrangements of  
79 chromosomes, collectively referred to as chromosome instability (CIN) <sup>1</sup>. CIN has been  
80 intimately associated with aneuploidy <sup>2</sup> and is one of the potential drivers of human genetic and  
81 neurodegenerative disorders <sup>3,4</sup>, aging <sup>5</sup> and several cancers <sup>6</sup>. While considered harmful for a cell  
82 or an organism, CIN may also contribute to generating variations and help in driving evolution,  
83 especially in unicellular primarily asexual eukaryotes <sup>7,8</sup>.

84

85 The current understanding of the mechanisms underlying genome stability has evolved through  
86 studies in a range of biological systems from unicellular yeasts to more complex metazoa  
87 including humans. These studies highlighted concerted actions of genes involved in (a) high-  
88 fidelity DNA replication and DNA damage repair, (b) efficient segregation of chromosomes and  
89 (c) error-correcting cellular surveillance machinery <sup>9,10</sup> in maintenance and inheritance of a stable  
90 genome. In recent years, large-scale screenings of loss-of-function <sup>11</sup>, reduction-of-function <sup>12</sup> and  
91 overexpression <sup>13,14,15,16</sup> mutant collections in the budding yeast *Saccharomyces cerevisiae* have  
92 appended the list of genome stability-regulators by identifying uncharacterized proteins as well as  
93 known proteins with functions in other cellular processes. However, considering the vast diversity  
94 of the chromosomal segregation mechanisms in eukaryotes, it is conceivable that many genes  
95 involved in genome maintenance are yet to be discovered and require additional screens in a wide  
96 range of organisms for their identification. While perturbation of a candidate gene's function to  
97 decipher its role in a cellular pathway has been a classical strategy in biological research,  
98 screening of strain collections aids in uncovering molecular players and cellular pathways in an  
99 unbiased manner.

100

101 The ascomycetous yeast *Candida albicans* is emerging as an attractive unicellular model for  
102 studying eukaryotic genome biology<sup>17</sup>. *C. albicans*, a commensal of both the gastrointestinal and  
103 genital tracts, remains the most frequently isolated fungal species worldwide from the patients  
104 diagnosed with candidemia or other nosocomial *Candida* infections<sup>18, 19</sup>. The diploid genome of  
105 *C. albicans* shows remarkable plasticity in terms of ploidy, single nucleotide polymorphism  
106 (SNP), loss of heterozygosity (LOH), copy number variations, and CIN events<sup>17, 20</sup>. Although  
107 LOH can be detected on all the chromosomes of *C. albicans*, the presence of recessive lethal or  
108 deleterious alleles on some haplotypes<sup>17</sup>, prevents one of the haplotypes or even a part of it from  
109 existing in the homozygous state. In particular, this homozygous bias has been observed for  
110 chromosomes R (ChR), 2 (Ch2), 4 (Ch4), 6 (Ch6) and 7 (Ch7)<sup>21, 22</sup>. LOH and aneuploidy-driven  
111 CIN has serious phenotypic consequences in *C. albicans* such as conferring resistance to  
112 antifungals<sup>23, 24, 25, 26, 27, 28</sup> or help *C. albicans* adapt to different host niches<sup>29, 30, 31</sup>. Whether  
113 genome plasticity is contributing to the success of *C. albicans* as a commensal or/and a dreaded  
114 pathogen of humans, remains an enigma<sup>17</sup>. Nevertheless, with increasing instances of *Candida*  
115 infections and emerging antifungal resistance, there is an immediate need to identify novel  
116 fungus-specific molecular targets that may aid the development of antifungal therapies. In  
117 addition, the remarkable ability of *C. albicans* to tolerate CIN in the form of whole chromosome  
118 loss, isochromosome formation, chromosome truncation, or mitotic crossing-over<sup>17, 20, 32</sup> raises  
119 intriguing questions on the functioning of genome stability-regulators in this fungal pathogen.

120  
121 Of utmost importance to maintain genomic integrity, is the efficient and error-free segregation of  
122 the replicated chromosomes. In most eukaryotes including *C. albicans*, the assembly of a  
123 macromolecular protein complex, called the kinetochore (KT), on CENP-A (Cse4 in budding  
124 yeasts) containing centromeric chromatin mediates chromosome segregation during mitosis<sup>33, 34</sup>,  
125<sup>35</sup>. The KT acts as a bridge between a chromosome and the connecting microtubules (MTs),  
126 emanating from the spindle pole bodies (SPBs), the functional homolog of centrosomes in  
127 mammals<sup>36</sup>. The subsequent attachment of sister KTs to opposite spindle poles then promotes the  
128 formation of a bipolar mitotic spindle that drives the separation of the duplicated chromosomes  
129 during anaphase<sup>37</sup>, after which cells exit mitosis and undergo cytokinesis<sup>38, 39, 40</sup>. In *C. albicans*,  
130 KT proteins remain clustered throughout the cell cycle and are shown to be essential for viability  
131 and mitotic progression<sup>33, 41, 42</sup>. In addition, genes involved in homologous recombination, such  
132 as *MRE11* and *RAD50*, and DNA damage checkpoint pathway, including *MEC1*, *RAD53* and  
133 *DUNI*, are required to prevent genome instability in *C. albicans*<sup>43, 44, 45</sup>. Strikingly, aberrant  
134 expression of proteins involved in DNA damage response or cell division triggers morphological

135 transition to a unique polarized, filamentous growth in *C. albicans*<sup>17</sup>. A recent screen, using a  
136 collection of 124 over-expression strains, has identified three additional genes, namely, *CDC20*,  
137 *BIMI*, and *RAD51*, with a role in genome maintenance as indicated by increased LOH-driven  
138 CIN upon overexpression in *C. albicans*<sup>46</sup>. Currently, only a minor fraction of the *C. albicans*  
139 gene armamentarium has been evaluated for their roles in genome stability. Systematic  
140 approaches are thus needed to exhaustively define the drivers of *C. albicans* genome maintenance  
141 and outline species-specific processes as well as commonalities with other eukaryotes.

142  
143 Here, we describe a large-scale screen aimed at identifying regulators of genome stability in a  
144 clinically relevant fungal model system. Our screen, involving ~20% of the *C. albicans*  
145 ORFeome, has identified Csa6, a yet unknown player of genome stability, as a critical regulator  
146 of cell cycle progression in *C. albicans*. Overall, this is the first-ever report of such a screen at this  
147 scale in *C. albicans* and provides a framework for identifying regulators of eukaryotic genome  
148 stability, some of which may serve as new targets for therapeutic interventions of fungal  
149 infections.

## 151 **Results**

### 153 **A reporter system for monitoring chromosome stability in *C. albicans***

154  
155 To understand the molecular mechanisms underlying genome instability in a fungal pathogen, we  
156 developed a reporter system in *C. albicans* in which whole chromosome loss can be distinguished  
157 from other events such as break-induced replication, gene conversion, chromosome truncation or  
158 mitotic crossing over<sup>22,46</sup>. In our prior work, a loss-of-heterozygosity (LOH) reporter strain was  
159 developed for use in *C. albicans*<sup>22,46</sup>. In this strain *GFP* and *BFP* genes, linked to *ARG4* and  
160 *HIS1* auxotrophic markers, respectively, are integrated at the same intergenic locus on the left  
161 arms of chromosome 4A (Ch4A) and chromosome 4B (Ch4B), respectively (Fig. **1A, S1A**)<sup>22</sup>.  
162 Consequently, cells express both GFP and BFP as analyzed by flow cytometry and are  
163 prototrophic for *ARG4* and *HIS1* genes, unless a chromosome instability (CIN) event causes loss  
164 of one of the two loci (Fig. **1A, B**)<sup>22</sup>. To differentiate whole chromosome loss from other events  
165 that may lead to loss of one of the two reporter loci, we modified the LOH reporter strain by  
166 integrating a red fluorescent protein (RFP) reporter gene, associated with the hygromycin B (hyg  
167 B) resistance marker, on the right arm of Ch4B (Fig. **1A, S1A**). The RFP reporter insertion is  
168 sufficiently distant from the BFP locus that loss of both BFP and RFP signal (and of their linked

169 auxotrophic/resistance markers) is indicative of loss of Ch4B, rather than a localized event  
170 causing loss of the *BFP-HIS1* reporter insertion (Fig. **1A, S1A**). Notably, while loss of Ch4A  
171 cannot be tolerated due to the presence of recessive lethal alleles on Ch4B<sup>22</sup>, loss of Ch4B leads  
172 to formation of small colonies that mature into larger colonies following duplication of Ch4A<sup>46</sup>.  
173 Thus, the absence of both *BFP-HIS1* and *RFP-HYG B* but continued presence of *GFP-ARG4* in  
174 the modified reporter strain, which we named as chromosome stability (CSA) reporter, enables us  
175 monitor loss of Ch4B in a population. The fluorescence intensity profile of GFP, BFP and RFP in  
176 the CSA reporter was validated by flow cytometry (Fig. **S1B**). To functionally validate the CSA  
177 reporter system, we employed overexpression of *CDC20*, a gene important for anaphase onset,  
178 activation of spindle assembly checkpoint and whose overexpression is known to cause whole  
179 chromosome loss in *C. albicans*<sup>46</sup>. We analyzed the BFP/GFP density plots in various control  
180 strains (Fig. **S1C**) and monitored the loss of BFP/GFP signal in cells overexpressing *CDC20*  
181 (*CDC20<sup>OE</sup>*) by flow cytometry. As reported earlier<sup>46</sup>, the *CDC20<sup>OE</sup>* strain displayed a higher  
182 population of BFP<sup>+</sup>GFP<sup>-</sup> and BFP<sup>-</sup>GFP<sup>+</sup> cells as compared to the empty vector (EV) control  
183 indicating increased CIN in the *CDC20<sup>OE</sup>* mutant (Fig. **S1D, E**). Next, we isolated BFP<sup>-</sup>GFP<sup>+</sup> cells  
184 of EV and *CDC20<sup>OE</sup>* using flow cytometry and plated them for subsequent analysis of  
185 auxotrophic/resistance markers (Fig. **S1F**). As noted above, upon incubation of the sorted BFP<sup>-</sup>  
186 GFP<sup>+</sup> cells, we observed the appearance of both small and large colonies (Fig. **S1F**). Small  
187 colonies have been previously shown to be the result of loss of Chr4B homolog and are predicted  
188 to be a consequence of Ch4A monosomy, eventually yielding large colonies upon reduplication of  
189 Ch4A<sup>46</sup>. We, therefore, performed the marker analysis on large colonies and found that 85% of  
190 the BFP<sup>-</sup>GFP<sup>+</sup> derived colonies of *CDC20<sup>OE</sup>* mutant concomitantly lost both *HIS1* and *HYG B* but  
191 retained *ARG4* (Fig. **S1G**) suggesting the loss of Ch4B homolog; flow cytometry analysis further  
192 confirmed the loss of BFP and RFP signals in these colonies. The remaining 15% of colonies  
193 retained *GFP-ARG4* and *RFP-HYG B* but not *BFP-HIS1* (Fig. **S1G**) indicating that more  
194 localized events including gene conversion, rather than whole chromosome loss, were responsible  
195 for loss of the BFP signals in these cells. The above data indicate that the CSA reporter system  
196 that we engineered enables precise monitoring of the whole chromosome loss event in a  
197 population and enables large-scale screening of this phenotype.

## 199 **Medium-throughput screening of *C. albicans* overexpression strains identifies regulators of** 200 **genome stability**

202 Systematic gene overexpression is an attractive approach for performing large-scale functional  
203 genomic analysis in *C. albicans*, a diploid ascomycete. Using a recently developed collection of  
204 *C. albicans* inducible overexpression plasmids (Chauvel et al., manuscript in preparation) and the  
205 CSA reporter strain described above, we generated a library of 1067 *C. albicans* inducible  
206 overexpression strains. Each of these strains, carrying a unique ORF under control of the  $P_{TET}$   
207 promoter, could be induced for overexpression after anhydrotetracycline (Atc) or doxycycline  
208 (Dox) addition (Fig. 1C)<sup>46,47</sup>. To identify regulators of genome stability, we carried out a primary  
209 screen with these 1067 overexpression strains by individually analyzing them for the loss of  
210 BFP/GFP signals by flow cytometry (Fig. 1C, S2A, Dataset 1). Our primary screening identified  
211 23 candidate genes (out of 1067) whose overexpression resulted in  $\geq 2$ -fold increase in the  
212 BFP<sup>+</sup>GFP<sup>-</sup> and BFP<sup>-</sup>GFP<sup>+</sup> population relative to the EV (Table S1, S2). Next, we carried out a  
213 secondary screen with these 23 overexpression strains to revalidate the loss of BFP/GFP markers  
214 by flow cytometry (Fig. 1C, S2B). As genotoxic stress is intimately linked with polarized growth  
215 in *C. albicans*<sup>17,48</sup>, we microscopically examined the overexpression strains exhibiting higher  
216 instability at the BFP/GFP locus during secondary screening for any morphological transition  
217 (Fig. 1C, S2B). While overexpression of 17 genes (out of 23) could not reproduce the BFP/GFP  
218 loss phenotype, overexpression of the six genes resulted in  $\geq 2$ -fold increase in the BFP<sup>+</sup>GFP<sup>-</sup> or  
219 BFP<sup>-</sup>GFP<sup>+</sup> population as compared to the EV, with three genes (out of 6) inducing polarized  
220 growth upon overexpression (Fig. S3A, B). These six genes, which we referred to as *CSA* genes,  
221 include *CSA1* (*CLB4*), *CSA2* (*ASE1*), *CSA3* (*KIP2*), *CSA4* (*MCM7*), *CSA5* (*BFA1*) and *CSA6*  
222 coded by *ORF19.1447* of unknown function (Fig. 1D).

223

### 224 **Molecular mechanisms underlying CIN in *CSA* overexpression mutants**

225

226 Out of the six *CSA* genes, overexpression of three genes, namely, *CSA1*<sup>*CLB4*</sup>, *CSA2*<sup>*ASE1*</sup> and  
227 *CSA3*<sup>*KIP2*</sup> caused little or no change in the morphology of *C. albicans* (Fig. S3A), but triggered  
228 CIN at the BFP/GFP locus, indicated by an expansion of the BFP<sup>+</sup>GFP<sup>-</sup> and BFP<sup>-</sup>GFP<sup>+</sup> population  
229 in the flow cytometry density plots (Fig. S3B, C). To further dissect the molecular mechanisms  
230 leading to the loss of BFP/GFP signals in these mutants, we sorted BFP<sup>-</sup>GFP<sup>+</sup> cells of these  
231 mutants and plated them for *GFP-ARG4*, *BFP-HIS1* and *RFP-HYG B* analysis, as described  
232 previously for the *CDC20*<sup>*OE*</sup> mutant. We observed that a majority of the large BFP<sup>-</sup>GFP<sup>+</sup> derived  
233 colonies of *CSA1*<sup>*CLB4*</sup>, *CSA2*<sup>*ASE1*</sup> and *CSA3*<sup>*KIP2*</sup> overexpression mutants lost *BFP-HIS1* but retained  
234 *RFP-HYG B* and *GFP-ARG4* (Fig. S3D), suggesting that localized genome instability events,

rather than whole chromosome loss events, contributed to the high percentage of BFP-GFP<sup>+</sup> cells in these mutants.

Overexpression of the remaining three genes, namely *CSA4*<sup>MCM7</sup>, *CSA5*<sup>BFA1</sup> and *CSA6*, drastically altered the morphology of the *C. albicans* cells by inducing polarized/filamentous growth (Fig. S3A). A connection between morphological switches and genotoxic stresses has been established in the polymorphic fungus *C. albicans*, wherein polarized growth is triggered in response to improper cell cycle regulation<sup>41, 42, 48, 49, 50</sup>. Flow cytometric analysis of cell cycle progression revealed that overexpression of *CSA4*<sup>MCM7</sup>, *CSA5*<sup>BFA1</sup> and *CSA6* shifted cells towards the 4N DNA content (Fig. S3E). To further determine the cell cycle phase associated with the 4N shift, we compared nuclear segregation patterns (Hoechst staining for DNA and CENP-A/Cse4 localization for KT) and spindle dynamics (separation of Tub4 foci) in these overexpression mutants with those of the EV control (Fig. S3F). Our results suggested the 4N shift in *CSA4*<sup>MCM7</sup> and *CSA6* overexpression mutants was a result of G2/M arrest, indicated by a high percentage of large-budded cells with unsegregated DNA mass and improperly separated SPBs (Fig. S3F). In contrast, the 4N shift upon *CSA5*<sup>BFA1</sup> overexpression was a consequence of late anaphase/telophase arrest, shown by an increased number of large-budded cells with segregated nuclei and SPBs (Fig. S3F). Taken together, our results indicate that the polarized growth in each of *CSA4*<sup>MCM7</sup>, *CSA5*<sup>BFA1</sup> and *CSA6* overexpression mutants is a probable outcome of improper cell cycle progression.

Two *CSA* genes, namely *CSA2*<sup>ASE1</sup> and *CSA5*<sup>BFA1</sup>, gave rise to similar overexpression phenotypes in both *S. cerevisiae* and *C. albicans* (Table 1). While phenotypes related to *CSA4*<sup>MCM7</sup> and *CSA6* overexpression in *S. cerevisiae* or other related organisms remained unreported, the overexpression phenotypes of the remaining *CSA* genes were along the lines of their roles in cell cycle functioning, as reported in *S. cerevisiae* (Table 1, Fig. 1D). Altogether, our results validated the role of *CSA* genes in regulating genome stability in *C. albicans*. While overexpression of either *CSA1*<sup>CLB4</sup>, *CSA2*<sup>ASE1</sup> or *CSA3*<sup>KIP2</sup> induced CIN mostly through non-chromosomal loss events, the effect of overexpression of either *CSA4*<sup>MCM7</sup>, *CSA5*<sup>BFA1</sup> or *CSA6* was so drastic that the *C. albicans* mutants were arrested at different cell cycle phases with G2/M equivalent DNA content (4N) and thus were unable to complete the mitotic cell cycle.

**Csa6 is an SPB-localizing protein, present across a subset of CUG-Ser clade fungal species**

269 Among the genes identified in the screen, Csa6 was the only protein without any detectable  
270 homolog in *S. cerevisiae* (Fig. 1D). This intrigued us to examine its presence across various other  
271 fungi. Phylogenetic analysis using high confidence protein homology searches and synteny-based  
272 analysis indicated that Csa6 is exclusively present in a subset of fungal species belonging to the  
273 CUG-Ser clade (Fig. 2A). Strikingly, in all these species, Csa6 was predicted to have a central  
274 coiled-coil domain (Fig. 2B). Epitope tagging of Csa6 with a fluorescent marker (mCherry)  
275 localized it close to the KT throughout the cell cycle in *C. albicans* (Fig. 2C). In most unicellular  
276 fungi, often found proximal to the clustered KTs, are the SPB complexes<sup>33, 35, 51, 52</sup>. Although  
277 neither the SPB structure nor its composition is well characterized in *C. albicans*, the majority of  
278 the SPB proteins exhibit high sequence and structural conservation from yeast to humans<sup>53</sup>.  
279 Hence, we re-examined Csa6 localization with two of the evolutionarily conserved SPB proteins,  
280 Tub4 and Spc110, in *C. albicans*<sup>53, 54</sup> (Fig. 2D, E). These results showed that Csa6 constitutively  
281 localizes to the SPBs, close to the KTs, in cycling yeast cells of *C. albicans* (Fig. 2D, E).

282

### 283 **Csa6, a previously uncharacterized protein, as a key regulator of mitotic progression in *C.*** 284 ***albicans***

285

286 While roles of Csa6 have not been investigated before, based on our findings thus far (Fig. S3E,  
287 F), we hypothesized that Csa6 plays an important function in cell cycle regulation and genome  
288 stability in *C. albicans*. We sought to identify the molecular pathways by which Csa6 performed  
289 its functions in *C. albicans*. We again made use of the inducible  $P_{TET}$  promoter system to generate  
290 a *CSA6*<sup>OE</sup> strain (CaPJ176, *P<sub>TET</sub>CSA6*) in the wild-type (SN148) background of *C. albicans* (Fig.  
291 3A). Conditional overexpression of TAP-tagged Csa6 (CaPJ181, *P<sub>TET</sub>CSA6-TAP*), in presence of  
292 Atc, was confirmed by western blot analysis (Fig. 3B). The effect of *CSA6*<sup>OE</sup> (CaPJ176,  
293 *P<sub>TET</sub>CSA6*) on cell cycle functioning was then investigated by flow cytometric cell cycle analysis  
294 (Fig. 3C) and microscopic examination of the nuclear division (Fig. 3D). As observed previously  
295 (Fig. S3E, F), *CSA6*<sup>OE</sup> inhibited cell cycle progression in *C. albicans* by arresting cells in the  
296 G2/M phase, evidenced by the gradual accumulation of large-budded cells with unsegregated  
297 nuclei (Fig. 3D), possessing 4N DNA content (Fig. 3C). Some of these large-budded cells also  
298 underwent a morphological transition to an elongated bud or other complex multi-budded  
299 phenotypes (Fig. 3D), indicating cell cycle arrest-mediated morphological switching<sup>48</sup> due to  
300 *CSA6*<sup>OE</sup>. Strikingly, continuous upregulation of Csa6 was toxic to the cells (Fig. S4A) as nuclei  
301 failed to segregate in this mutant (Fig. 3D).

302

303 Nuclear segregation during mitosis is facilitated by the formation of the mitotic spindle and its  
304 dynamic interactions with chromosomes via KTs. Thus, we sought to examine both the KT  
305 integrity and the mitotic spindle morphology in the *CSA6<sup>OE</sup>* mutants. In *C. albicans*, the structural  
306 stability of the KT is a determinant of CENP-A/Cse4 stability wherein depletion of any of the  
307 essential KT proteins results in delocalization and degradation of the CENP-A/Cse4 by ubiquitin-  
308 mediated proteolysis<sup>50</sup>. Fluorescence microscopy and western blot analysis confirmed that Cse4  
309 was neither delocalized (Fig. **S4B**) nor degraded from centromeric chromatin (Fig. **S4C**) upon  
310 *CSA6<sup>OE</sup>*. Next, we analyzed the spindle integrity in *CSA6<sup>OE</sup>* mutants by tagging Tub4 (SPB) and  
311 Tub1 (MTs) with fluorescent proteins. Fluorescence microscopy analysis revealed that a large  
312 proportion (~73%) of the large-budded cells formed an unconventional rudimentary mitotic  
313 spindle structure upon *CSA6<sup>OE</sup>*, wherein it had a dot-like appearance as opposed to an elongated  
314 bipolar rod-like spindle structure in EV or uninduced (-Atc) strains (Fig. **3E**). This suggests that  
315 nuclear segregation defects in *CSA6<sup>OE</sup>* mutant cells are an attribute of aberrant mitotic spindle  
316 formation that might have led to the mitotic arrest.

317  
318 During mitosis, surveillance mechanisms, including spindle assembly checkpoint (SAC)<sup>55,56</sup> and  
319 spindle positioning checkpoint (SPOC)<sup>57,58</sup> operate to maintain genome stability by delaying the  
320 metaphase-anaphase transition in response to improper chromosome-spindle attachments and  
321 spindle misorientation, respectively. We posit that the G2/M cell cycle arrest due to *CSA6<sup>OE</sup>* in *C.*  
322 *albicans* could be a result of either SAC or SPOC activation. Hence, we decided to inactivate  
323 SAC and SPOC, individually, in the *CSA6<sup>OE</sup>* strain by deleting the key spindle checkpoint genes  
324 *MAD2*<sup>41</sup> and *BUB2*<sup>48</sup>, respectively. SAC inactivation in *CSA6<sup>OE</sup>* mutant cells (Fig. **4A**) led to the  
325 emergence of unbudded cells with 2N DNA content (Fig. **4B, C**), indicating a bypass of the G2/M  
326 arrest caused by *CSA6<sup>OE</sup>*. Consequently, we also observed a partial rescue of the growth defect in  
327 *CSA6<sup>OE</sup>* mutant cells (Fig. **S5A**). Next, we sought to characterize the effect of SAC inactivation  
328 on the spindle integrity in *CSA6<sup>OE</sup>* mutants. *CSA6<sup>OE</sup>* resulted in the formation of an  
329 unconventional mitotic spindle (Fig. **3E**) wherein it displayed a single focus of SPB (Tub4-GFP),  
330 colocalizing with a single focus of MTs (Tub1-mCherry). We speculated two possibilities that  
331 may lead to the single focus of Tub4: a) a defect in the process of SPB duplication or b) a delay in  
332 the separation of duplicated SPBs. Fluorescence microscopy analysis revealed that SAC  
333 inactivation in *CSA6<sup>OE</sup>* mutant drastically increased the percentage of large-budded cells (from  
334 ~30% to ~68%) with two separated SPB foci (Tub4-GFP) (Fig. **S5B**). These results ruled out the  
335 possibility of an unduplicated SPB in *CSA6<sup>OE</sup>* mutant cells and hinted at the importance of  
336 cellular Csa6 levels for proper SPB separation and chromosome segregation in *C. albicans*.

337  
338  
339  
340  
341  
342  
343  
344  
345  
346  
347  
348  
349  
350  
351  
352  
353  
354  
355  
356  
357  
358  
359  
360  
361  
362  
363  
364  
365  
366  
367  
368  
369

We next determined the effect of inactivating SPOC in the cells overexpressing Csa6. For this, we generated a *CSA6<sup>OE</sup>* strain (CaPJ200) using the *bub2* null mutant (CaPJ110) as the parent strain and monitored nuclear division following Hoechst staining. Strikingly, we did not observe a bypass of G2/M arrest in *CSA6<sup>OE</sup>* mutant upon SPOC inactivation, indicated by a persistent population of large-budded cells with unsegregated nuclei (Fig. **S5C**). Altogether, our results demonstrate that overexpression of Csa6 leads to a Mad2-mediated metaphase arrest due to a malformed spindle in *C. albicans*.

### **Csa6 regulates mitotic exit network and is essential for viability in *C. albicans***

To further gain insights into the biological function of Csa6, we sought to generate a promoter shut-down mutant of *csa6* (*CSA6<sup>PSD</sup>*). For this, we deleted one of its alleles and placed the remaining one under the control of the *MET3* promoter<sup>59</sup> which gets repressed in presence of methionine (Met/M) and cysteine (Cys/C) (Fig. **5A**). Western blot analysis confirmed the depletion of TAP-tagged Csa6 in *CSA6<sup>PSD</sup>* mutant within 6 h of growth under repressive conditions (Fig. **5B**). The inability of *CSA6<sup>PSD</sup>* mutant to grow in non-permissive conditions confirmed the essentiality of Csa6 for viability in *C. albicans* (Fig. **5C**). Subsequently, we analyzed the cell cycle profile (Fig. **5D**) and nuclear division dynamics (Fig. **5E**) in the *CSA6<sup>PSD</sup>* strain after a specific period of incubation in either permissive or non-permissive conditions. Strikingly, Csa6 depletion, as opposed to its overexpression, resulted in cell cycle arrest at the late anaphase/telophase stage, indicated by an increasing proportion of large-budded cells, possessing segregated nuclei and 4N DNA content (Fig. **5D, E**). Additionally, we observed cells with more than two nuclei, elongated-budded cells and other complex phenotypes upon Csa6 depletion (Fig. **5E**). While CENP-A/Cse4 remained localized to centromeres in *CSA6<sup>PSD</sup>* mutant as revealed by the fluorescence microscopy (Fig. **S6A**), an increase in the cellular levels of Cse4 was observed in *CSA6<sup>PSD</sup>* mutant by western blot analysis (Fig. **S6B**). The increase in Cse4 levels could be an outcome of Cse4 loading at anaphase in *C. albicans*<sup>60,61</sup>. Finally, we analyzed the integrity of the mitotic spindle, as mentioned previously, in *CSA6<sup>PSD</sup>* mutant. We noticed the mean length of the anaphase mitotic spindle in Csa6-depleted cells was significantly higher (~11  $\mu$ m) than that of the cells grown under permissive conditions (~6  $\mu$ m), indicating a spindle disassembly defect in *CSA6<sup>PSD</sup>* mutant (Fig. **5F**).

370 A close link between anaphase arrest, hyper-elongated mitotic spindle and inactive mitotic exit  
371 network (MEN) have been established before <sup>40, 62, 63</sup>. Localized at the SPB, the MEN is a  
372 signaling cascade in *S. cerevisiae* that triggers cells to come out of mitosis and proceed to  
373 cytokinesis (Fig. 6A) <sup>64</sup>. We speculated the anaphase arrest in *CSA6<sup>PSD</sup>* mutant could be a result of  
374 an inactive MEN signaling. To determine this, we sought to bypass the anaphase arrest associated  
375 with Csa6 depletion by overexpressing *SOL1*, the CDK inhibitor and Sic1 homolog in *C. albicans*  
376 <sup>65</sup> (Fig. 6B), using the inducible *P<sub>TET</sub>* system mentioned previously (Fig. 6C). The conditional  
377 overexpression of Protein A-tagged Sol1 upon addition of Atc was verified by western blot  
378 analysis (Fig. 6D). Strikingly, *SOL1<sup>OE</sup>* in association with Csa6 depletion allowed cells to exit  
379 mitosis but not cytokinesis, as evidenced by the formation of chains of cells with >4N DNA  
380 content (Fig. 6E, F). To further examine the role of Csa6 in mitotic exit, we analyzed the  
381 localization of a MEN component, Tem1, a GTPase that is known to initiate MEN signaling <sup>39, 66,</sup>  
382 <sup>67, 68</sup>. In *C. albicans*, Tem1 localizes to SPBs in a cell-cycle-regulated manner and is essential for  
383 viability <sup>39</sup>. Fluorescence microscopy revealed that while Tem1 is localized to both the SPBs in  
384 anaphase under permissive conditions (Fig. 6G) as observed earlier <sup>39</sup>, a high percentage of Csa6-  
385 depleted cells (~78%) had Tem1 localized to only one of the two SPBs (Fig. 6G), suggesting an  
386 important role of Csa6 in regulating mitotic exit in *C. albicans*. Altogether, our results  
387 demonstrate that Csa6 is required for mitotic exit and thus essential for viability in *C. albicans*.

388

### 389 **Csa6 of *Candida dubliniensis* functionally complements Csa6 of *C. albicans***

390

391 To further elucidate the intra-species function and localization of Csa6, we decided to ectopically  
392 express Csa6 of another CUG-Ser clade species, *Candida dubliniensis* (CdCsa6) in *C. albicans*.  
393 *C. dubliniensis* is a human pathogenic budding yeast that shares a high degree of DNA sequence  
394 homology with *C. albicans*, and possesses unique and different centromere DNA sequences on  
395 each of its eight chromosomes <sup>69, 70</sup>. Upon protein sequence alignment, we found that CdCsa6  
396 (*ORF Cd36\_16290*) is 79% identical to Csa6 of *C. albicans* (CaCsa6) (Fig. 7A). The ectopic  
397 expression of GFP-tagged CdCsa6 in *C. albicans* was carried out using the replicative plasmid  
398 pCdCsa6-GFP-ARS2 (Fig. 7B), which contains the autonomously replicating sequence (ARS) of  
399 *C. albicans* <sup>71</sup>. Although unstable when present in an episomal form, ARS plasmids, upon  
400 spontaneous integration into the genome, can propagate stably over generations <sup>72</sup>. Fluorescence  
401 microscopy of integrated pCdCsa6-GFP-ARS2 revealed that similar to CaCsa6, CdCsa6 localizes  
402 constitutively to the SPBs in *C. albicans* (Fig. 7C), further supporting Csa6's evolutionarily  
403 conserved role in regulating mitotic spindle and mitotic exit in *C. albicans*. We next asked if

404 CdCsa6 can functionally complement CaCsa6. For this, we ectopically expressed CdCsa6 in  
405 *CSA6<sup>PSD</sup>* strain. Strikingly, the ectopic expression of CdCsa6 rescued the growth defect associated  
406 with *CSA6<sup>PSD</sup>* mutant under non-permissive conditions, indicating CdCsa6 can functionally  
407 complement CaCsa6 (Fig. 7D). This suggests functional conservation of Csa6 among related  
408 *Candida* species belonging to the CUG-Ser clade.

409

## 410 Discussion

411

412 In this study, we carried out an extensive screen to identify genes that contribute to genome  
413 stability in *C. albicans* by generating and analyzing a library of more than a thousand  
414 overexpression strains. Our screen identified six regulators of chromosome stability including  
415 Csa6, a protein of unknown function. Molecular dissection of Csa6 function revealed its  
416 importance in cell cycle progression at least in two critical stages, metaphase-anaphase transition  
417 and mitotic exit. We further demonstrated that Csa6 is constitutively localized to the SPBs,  
418 essential for viability, and alterations of its cellular level leads to cell cycle arrest in *C. albicans*.  
419 Finally, subcellular localization and complementation analysis revealed functional conservation  
420 of Csa6 across the pathogenic *Candida* species.

421

422 The identification of two *CSA* genes, *CSA2<sup>ASE1</sup>* and *CSA5<sup>BFA1</sup>*, that were earlier reported as CIN  
423 genes<sup>13, 14</sup>, further validates the power of the screening approach and the methods presented in  
424 this study. The respective overexpression phenotypes of these two genes in *C. albicans* were  
425 found to be similar to those in *S. cerevisiae*, suggesting that their functions might be conserved in  
426 these distantly related yeast species. In *S. cerevisiae*, Ase1 acts as an MT-bundling protein,  
427 required for spindle elongation and stabilization during anaphase<sup>73, 74</sup> (Fig. 8A). Hence, increased  
428 CIN upon *ASE1* overexpression might be an outcome of premature spindle elongation and  
429 improper KT-microtubule attachments<sup>74, 75</sup>. Bfa1, on the other hand, is a key component of the  
430 Bub2-Bfa1 complex, involved in SPOC activation<sup>57</sup>, and a negative regulator of mitotic exit<sup>76</sup>  
431 (Fig. 8A). In *S. cerevisiae*, *BFA1* overexpression prevents Tem1 from interacting with its  
432 downstream effector protein Cdc15, thus inhibiting MEN signaling and arresting cells at the  
433 anaphase<sup>77</sup>. In our screen, a B-type mitotic cyclin Clb4 (*CSA1*), and a kinesin-related motor  
434 protein Kip2 (*CSA3*) (Fig. 8A), were found to increase CIN upon overexpression, primarily via  
435 non-chromosomal loss events. *C. albicans* Clb4 acts as a negative regulator of polarized growth<sup>49</sup>  
436 and is the functional homolog of *S. cerevisiae* Clb5<sup>78</sup>, required for the entry into the S-phase<sup>79</sup>.  
437 Increased CIN upon *CSA1<sup>CLB4</sup>* overexpression, is thus consistent with its role in S-phase initiation.

438 The function of Kip2, however, is yet to be characterized in *C. albicans*. In *S. cerevisiae*, Kip2  
439 functions as an MT polymerase<sup>80</sup>, with its overexpression leading to hyperextended MTs and  
440 defects in SPB separation<sup>81</sup>. The associated CIN observed upon *CSA3*<sup>KIP2</sup> overexpression in *C.*  
441 *albicans* is in line with its function in nuclear segregation.

442  
443 Mcm7, another *CSA* gene (*CSA4*) identified in this study, is a component of the highly conserved  
444 Mcm2-7 helicase complex, essential for eukaryotic DNA replication initiation and elongation<sup>82</sup>  
445 (Fig. 8A). While Mcm7 depletion arrests cells at S phase<sup>83</sup>, the effect of *MCM7* overexpression  
446 on genomic integrity is comparatively less explored. Especially, several cancerous cells have been  
447 shown to overexpress Mcm7<sup>84,85,86</sup>, with its elevated levels increasing the chances of relapse and  
448 local invasions<sup>84</sup>. In this study, we found that overexpression of *MCM7*, in contrast to Mcm7  
449 depletion, arrested cells at the G2/M stage. One possibility is increased Mcm7 levels interfered  
450 with DNA replication during the S phase, resulting in DNA damage or accumulation of single-  
451 stranded DNA, thus activating the *RAD9*-dependent cell cycle arrest at the G2/M stage<sup>87,88</sup>. In a  
452 recent study from our laboratory, Mcm7 has been identified as a subunit of the kinetochore  
453 interactome in a basidiomycete yeast *Cryptococcus neoformans*<sup>89</sup>. Another subunit of the Mcm2-  
454 7 complex, Mcm2, is involved in regulating the stability of centromeric chromatin in *C. albicans*  
455<sup>61</sup>. Considering the growing evidence of the role of Mcm2-7 subunits beyond their canonical,  
456 well-established roles in DNA replication, the serendipitous identification of Mcm7 as a regulator  
457 of genome stability in our screen is striking.

458  
459 We performed an in-depth analysis of *Csa6*, a novel regulator of cell cycle progression identified  
460 from our screen (Fig. 8B, C). Our results revealed that overexpression of *CSA6* leads to an  
461 unconventional mitotic spindle formation and SAC-dependent G2/M cell cycle arrest (Fig. 8C) in  
462 *C. albicans*. While *mad2* deletion indicated that SPB duplication and separation of duplicated  
463 SPBs is unperturbed in *CSA6* overexpressing cells, what exactly triggered the activation of SAC  
464 in these cells remains to be determined. Recent studies on human cell lines have shown that  
465 failure in the timely separation of the centrosomes promotes defective chromosome-MT  
466 attachments and may lead to chromosome lagging if left uncorrected by the cellular surveillance  
467 machinery<sup>90,91,92</sup>. Along the same lines, we posit that a delay in SPB separation, mediated by  
468 overexpression of *Csa6*, leads to increased instances of improper chromosome-MT attachments,  
469 leading to SAC activation and an indefinite arrest at the metaphase stage. Future studies on the  
470 SPB structure-function and composition in *C. albicans* should reveal how *Csa6* regulates SPB  
471 dynamics in this organism.

472

473 In contrast to its overexpression, Csa6 depleted cells failed to exit mitosis and remained arrested  
474 at the late anaphase/telophase stage (Fig. **8C**). We further linked the mitotic exit failure in Csa6  
475 depleted cells with the defective localization of Tem1, an upstream MEN protein. While the  
476 hierarchy of MEN components, starting from the MEN scaffold Nud1, an SPB protein, to its  
477 ultimate effector Cdc14 is well established in *S. cerevisiae*<sup>64</sup>, the existence of a similar hierarchy  
478 in *C. albicans* needs to be investigated. In addition, several lines of evidence suggest that MEN in  
479 *C. albicans* may function differently from *S. cerevisiae*: (a) Unlike *S. cerevisiae*, *C. albicans*  
480 Cdc14 is non-essential for viability with its deletion affecting cell separation<sup>93</sup>. (b) Cdc14 is  
481 present in the nucleoplasm for the majority of the cell cycle in contrast to its nucleolar  
482 localization in *S. cerevisiae*<sup>93</sup>. (c) *C. albicans* Dbf2 is required for proper nuclear segregation,  
483 actomyosin ring contraction, and cytokinesis<sup>38</sup>. A recent study involving the identification of  
484 Cdc14 interactome in *C. albicans*<sup>94</sup> found only a subset of proteins (0.2%) as physical or genetic  
485 interactors in *S. cerevisiae*, suggesting the divergence of Cdc14 functions in *C. albicans*. Hence,  
486 further investigations of MEN functioning in *C. albicans* are required to understand its divergence  
487 from *S. cerevisiae* and the mechanism by which Csa6 regulates mitotic exit in *C. albicans* and  
488 related species. Altogether, our results indicate that Csa6 has dual functions during cell cycle  
489 progression wherein it is first required during the G2/M phase for proper assembly of the mitotic  
490 spindle and then later during anaphase to exit the cells from mitosis. In addition, the constitutive  
491 localization of Csa6 to the SPBs strengthens the link between SPB-related functions and Csa6 in  
492 *C. albicans* (Fig. **8B, C**).

493

494 The phylogenetic analysis of Csa6 revealed that it is only present in a group of fungal species,  
495 belonging to the CUG-Ser clade. Combined with its essential cell-cycle-related functions, it is  
496 intriguing to determine whether emergence of Csa6 is required to keep the pace of functional  
497 divergence in the regulatory mechanisms of cell cycle progression in these *Candida* species.  
498 While we demonstrated Csa6 of *C. dubliniensis* functionally complements Csa6 of *C. albicans*,  
499 whether Csa6 of distant species can also functionally complement CaCsa6 remains to be  
500 investigated. A recent study shows that around 50 essential genes, including Csa6, are only  
501 present in a group of *Candida* species (see Dataset 5 in<sup>95</sup>). Identification and functional  
502 characterization of these genes in the future will aid in developing clade-specific antifungal  
503 therapies<sup>95</sup>. In this study, we have analyzed only a part of the *C. albicans* ORFeome for their  
504 roles in genome maintenance. Further screening of the remaining overexpression ORFs will

505 provide a complete network of the molecular pathways regulating genome stability in human  
506 fungal pathogens.

## 508 **Materials and Methods**

509  
510 **1. Strains, plasmids and primers.** Information related to strains, plasmids and primers used in  
511 this study is available in the supplementary material.

512  
513 **2. Media and growth conditions.** *C. albicans* strains were routinely grown at 30°C in YPD (1%  
514 yeast extract, 2% peptone, 2% dextrose) medium supplemented with uridine (0.1 µg/ml) or  
515 complete medium (CM, 2% dextrose, 1% yeast nitrogen base and auxotrophic supplements) with  
516 or without uridine (0.1 µg/ml) and amino acids such as histidine, arginine, leucine (0.1 µg/ml).  
517 Solid media were prepared by adding 2% agar. For the selection of transformants, nourseothricin  
518 and hygromycin B (hyg B) were used at a final concentration of 100 µg/ml and 800 µg/ml,  
519 respectively, in the YPDU medium.

520  
521 Overexpression of genes from the tetracycline inducible promoter ( $P_{TET}$ ) was achieved by the  
522 addition of anhydrotetracycline (Atc, 3 µg/ml) or doxycycline (Dox, 50 µg/ml) in YPDU medium  
523 at 30°C<sup>47</sup> in the dark as Atc and Dox are light-sensitive. The *CSA6<sup>PSD</sup>* strains were grown at 30°C  
524 either in permissive (YPDU) or nonpermissive (YPDU + 5mM methionine (M) + 5mM cysteine  
525 (C)) conditions of the *MET3* promoter<sup>59, 61</sup>. *E. coli* strains were cultured at 30°C or 37°C in  
526 Luria-Bertani (LB) medium or 2YT supplemented with ampicillin (50 µg/ml or 100 µg/ml),  
527 chloramphenicol (34 µg/ml), kanamycin (50 µg/ml) and tetracycline (10 µg/ml). Solid media  
528 were prepared by adding 2% agar. Chemically competent *E. coli* cells were prepared according to  
529 Chung *et al*<sup>96</sup>.

530  
531 **3. Flow cytometry analysis.** Cultures of overexpression strains following 8 h of induction in  
532 YPDU+Atc and overnight recovery in the YPDU medium alone, were diluted in 1x phosphate-  
533 buffered saline (PBS) and analyzed (~10<sup>6</sup> cells) for the BFP/GFP marker by flow cytometry  
534 (FACSAria III, BD Biosciences) at a rate of 7000-10,000 events/s. We used 405- and 488-nm  
535 lasers to excite the BFP and GFP fluorophores and 450/40 and 530/30 filters to detect the BFP  
536 and GFP emission signals, respectively.

538 **4. Primary and secondary overexpression screening.** To detect CIN at the BFP/GFP locus  
539 upon  $P_{TET}$  activation, overnight grown cultures of *C. albicans* overexpression strains were  
540 reinoculated in CM-His-Arg to ensure all cells contained *BFP-HIS1* or *GFP-ARG4*. To measure  
541 the loss of BFP/GFP signals in 96-well plates, a *CDC20<sup>OE</sup>* mutant was used as a positive control.  
542 The primary selection of the overexpression mutants with increased  $BFP^+GFP^-$  and  $BFP^-GFP^+$   
543 cells was done by determining the BFP/GFP loss frequency in EV. For this, we analyzed the flow  
544 cytometry density plots for 22 independent cultures of EV using the FlowJo software (FlowJo X  
545 10.0.7r2). We observed a similar profile for all the cultures. We then defined gates for the  
546  $BFP^+GFP^-$  and  $BFP^-GFP^+$  fractions of cell population in one of the EV samples and applied these  
547 gates to the rest of EV samples. The mean frequency of  $BFP^+GFP^-$  and  $BFP^-GFP^+$  cells in EV was  
548 calculated (Table S1). Similar gates were applied to all 1067 overexpression strains analyzed for  
549 BFP/GFP markers and the frequency of  $BFP^+GFP^-$  and  $BFP^-GFP^+$  cells for each strain was  
550 determined (Dataset 1). The overexpression mutants, in which the BFP/GFP loss frequency was  
551  $\geq 2$ -fold than EV, were selected for further analysis (Table S2).

552  
553 For secondary screening, the overexpression plasmids present in each of the overexpression  
554 strains, identified from the primary screen (23 out of 1067), were used to retransform the CSA  
555 reporter strain (CEC5201). The overexpression strains (23) were analyzed by flow cytometry to  
556 revalidate the loss of BFP/GFP signals. Overexpression strains displaying  $\geq 2$ -fold higher  
557 frequency of  $BFP^+GFP^-/BFP^-GFP^+$  population than EV (6 out of 23) were monitored for any  
558 morphological transition by microscopy. As filamentous morphotype could distort the BFP/GFP  
559 loss analysis<sup>46</sup>, we characterized the overexpression mutants exhibiting increased CIN at the  
560 BFP/GFP locus and filamentous growth (3 out of 6) by monitoring cell cycle progression. For  
561 this, we transformed the overexpression plasmids in CaPJ159 and analyzed the overexpression  
562 strains (*CSA4<sup>MCM7</sup>*, *CSA5<sup>BFA1</sup>* and *CSA6*) for DNA content, nuclear segregation and SPB  
563 separation. The 6 genes identified from the secondary screen were verified for the correct *C.*  
564 *albicans* ORF by Sanger sequencing using a common primer PJ90. During the secondary  
565 screening, we also cultured overexpression mutants in YPDU without Atc and observed no  
566 differences between EV and uninduced (-Atc) cultures in terms of morphology and the BFP/GFP  
567 loss frequency.

568  
569 **5. Cell sorting and marker analysis following a CIN event.** Overnight grown cultures of EV  
570 and overexpression mutants (*CDC20*, *CSA1<sup>CLB4</sup>*, *CSA2<sup>ASE1</sup>* and *CSA3<sup>KIP2</sup>*) were reinoculated in  
571 YPDU+Atc for 8 h and allowed to recover overnight in YPDU-Atc. The cultures were analyzed

572 for BFP/GFP loss by flow cytometry followed by fluorescence-activated cell sorting (FACS)  
573 using a cell sorter (FACSAria III, BD Biosciences) at a rate of 10,000 events/s. Approximately  
574 1500 cells from the BFP<sup>-</sup>GFP<sup>+</sup> population were collected into 1.5-ml tubes containing 400  $\mu$ l  
575 YPDU and immediately plated onto YPDU agar plates. Upon incubation at 30°C for 2 days, both  
576 small and large colonies appeared, as reported earlier (46). As most small colonies are expected to  
577 have undergone loss of the Ch4B haplotype (46), we analyzed auxotrophic/resistance markers of  
578 large colonies to characterize the molecular mechanisms underlying CIN in the overexpression  
579 mutants.

580

581 For marker analysis, we replica plated the large colonies along with the appropriate control strains  
582 on CM-Arg, CM-His and YPDU+hyg B (800  $\mu$ g/ml) and incubated the plates at 30°C for 2 days.  
583 The colonies from CM-Arg plates were then analyzed for BFP, GFP and RFP markers by flow  
584 cytometry. For this, overnight grown cultures in YPDU were diluted in 1x PBS and 5000-10,000  
585 cells were analyzed (FACSAria III, BD Biosciences). We used 405-, 488- and 561 nm lasers to  
586 excite the BFP, GFP and RFP fluorophores and 450/40, 530/30, 582/15 filters to detect the BFP,  
587 GFP and RFP emission signals, respectively.

588

589 **6. Cell cycle analysis.** Overnight grown cultures of *C. albicans* were reinoculated at an OD<sub>600</sub> of  
590 0.2 in different media (as described previously) and harvested at various time intervals post-  
591 inoculation (as mentioned previously). The overnight grown culture itself was taken as a control  
592 sample (0 h) for all the experiments. Harvested samples were processed for propidium iodide (PI)  
593 staining as described before<sup>33</sup>. Stained cells were diluted to the desired cell density in 1x PBS and  
594 analyzed ( $\geq$ 30, 000 cells) by flow cytometry (FACSAria III, BD Biosciences) at a rate of 250-  
595 1000 events/s. The output was analyzed using the FlowJo software (FlowJo X 10.0.7r2). We used  
596 561-nm laser to excite PI and 610/20 filter to detect its emission signals.

597

598 **7. Fluorescence microscopy.** For nuclear division analysis in untagged strains, the *C. albicans*  
599 cells were grown overnight. The next day, the cells were transferred into different media (as  
600 mentioned previously) with a starting O.D.<sub>600</sub> of 0.2, collected at various time intervals (as  
601 described previously) and fixed with formaldehyde (3.7%). Cells were pelleted and washed thrice  
602 with 1x PBS, and Hoechst dye (50 ng/ml) was added to the cell suspension before imaging.  
603 Nuclear division in Cse4- and Tub4-tagged strains was analyzed as described above, except the  
604 cells were not fixed with formaldehyde. For Tem1 and mitotic spindle localization, overnight  
605 grown cultures were transferred to different media (as mentioned previously) with a starting

606 O.D.<sub>600</sub> of 0.2 and were grown for 6 h or 8 h. Cells were then washed, resuspended in 1x PBS and  
607 imaged on a glass slide. Localization studies of each, CaCsa6, Tub4, Spc110 and CdCsa6 was  
608 carried out by washing the log phase grown cultures with 1x PBS (three times) followed by image  
609 acquisition.

610  
611 The microscopy images were acquired using fluorescence microscope (Zeiss Axio Observer 7  
612 equipped with Colibri 7 as the LED light source), 100x Plan Apochromat 1.4 NA objective, pco.  
613 edge 4.2 sCMOS. We used Zen 2.3 (blue edition) for image acquisition and controlling all  
614 hardware components. Filter set 92 HE with excitation 455–483 and 583–600 nm for GFP and  
615 mCherry, respectively, and corresponding emission was captured at 501–547 and 617–758 nm. Z  
616 sections were obtained at an interval of 300 nm. All the images were displayed after the maximum  
617 intensity projection using ImageJ. Image processing was done using ImageJ. We used the cell  
618 counter plugin of ImageJ to count various cell morphologies in different mutant strains. Images  
619 acquired in the mCherry channel were processed using the subtract background plugin of ImageJ  
620 for better visualization.

621  
622 **8. Protein preparation and western blotting.** Approximately 3 O.D.<sub>600</sub> equivalent cells were  
623 taken, washed with water once and resuspended in 12.5% TCA (trichloroacetic acid) and  
624 incubated at -20°C overnight for precipitation. The cells were pelleted down and washed twice  
625 with ice-cold 80% acetone. The pellet was then allowed to air dry and finally resuspended in lysis  
626 buffer (0.1N NaOH and 1% SDS and 5xprotein loading dye). Samples were boiled at 95°C for 5-  
627 10 min and electrophoresed on a 10% SDS polyacrylamide gel. Gels were transferred to a  
628 nitrocellulose membrane by semi-dry method for 30 min at 25V and blocked for an hour in 5%  
629 non-fat milk in 1x PBS. Membranes were incubated with a 1:5000 dilution of rabbit anti-Protein  
630 A or mouse anti-PSTAIRE in 2.5% non-fat milk in 1x PBS. Membranes were washed three times  
631 in 1x PBS-Tween (0.05%) and then exposed to a 1:10,000 dilution of either anti-mouse- or anti-  
632 rabbit-IgG horseradish peroxidase antibody in 2.5% non-fat milk in 1x PBS. Membranes were  
633 washed three times in 1x PBS-Tween (0.05%) and developed using chemiluminescence method.

634  
635 **9. Statistical analysis.** Statistical significance of differences was calculated as mentioned in the  
636 figure legends with unpaired one-tailed *t*-test, paired one-tailed *t*-test, paired two-tailed *t*-test or  
637 one-way ANOVA with Bonferroni posttest. *P*-values  $\geq 0.05$  were considered as nonsignificant  
638 (n.s.). *P*-values of the corresponding figures are mentioned, if significant. All analyses were  
639 conducted using GraphPad Prism version Windows v5.00.

640  
641  
642  
643  
644  
645  
646  
647  
648  
649  
650  
651  
652  
653  
654  
655  
656  
657  
658  
659  
660  
661  
662  
663  
664  
665  
666  
667  
668  
669  
670  
671  
672  
673  
674  
675  
676  
677  
678  
679  
680  
681  
682  
683  
684  
685  
686  
687  
688

## References

1. Aguilera A, Gomez-Gonzalez B. Genome instability: a mechanistic view of its causes and consequences. *Nat Rev Genet* **9**, 204-217 (2008).
2. Potapova TA, Zhu J, Li R. Aneuploidy and chromosomal instability: a vicious cycle driving cellular evolution and cancer genome chaos. *Cancer Metastasis Rev* **32**, 377-389 (2013).
3. Yurov YB, Vorsanova SG, Iourov IY. Chromosome Instability in the Neurodegenerating Brain. *Front Genet* **10**, 892 (2019).
4. Taylor AMR, *et al.* Chromosome instability syndromes. *Nat Rev Dis Primers* **5**, 64 (2019).
5. Petr MA, Tulika T, Carmona-Marin LM, Scheibye-Knudsen M. Protecting the Aging Genome. *Trends Cell Biol* **30**, 117-132 (2020).
6. Negrini S, Gorgoulis VG, Halazonetis TD. Genomic instability--an evolving hallmark of cancer. *Nat Rev Mol Cell Biol* **11**, 220-228 (2010).
7. Guin K, *et al.* Spatial inter-centromeric interactions facilitated the emergence of evolutionary new centromeres. *Elife* **9**, (2020).
8. Sankaranarayanan SR, *et al.* Loss of centromere function drives karyotype evolution in closely related *Malassezia* species. *Elife* **9**, (2020).
9. Aguilera A, Garcia-Muse T. Causes of genome instability. *Annu Rev Genet* **47**, 1-32 (2013).
10. Levine MS, Holland AJ. The impact of mitotic errors on cell proliferation and tumorigenesis. *Genes Dev* **32**, 620-638 (2018).
11. Yuen KW, Warren CD, Chen O, Kwok T, Hieter P, Spencer FA. Systematic genome instability screens in yeast and their potential relevance to cancer. *Proc Natl Acad Sci U S A* **104**, 3925-3930 (2007).
12. Stirling PC, *et al.* The complete spectrum of yeast chromosome instability genes identifies candidate CIN cancer genes and functional roles for ASTRA complex components. *PLoS Genet* **7**, e1002057 (2011).
13. Stevenson LF, Kennedy BK, Harlow E. A large-scale overexpression screen in *Saccharomyces cerevisiae* identifies previously uncharacterized cell cycle genes. *Proc Natl Acad Sci U S A* **98**, 3946-3951 (2001).
14. Duffy S, *et al.* Overexpression screens identify conserved dosage chromosome instability genes in yeast and human cancer. *Proc Natl Acad Sci U S A* **113**, 9967-9976 (2016).

- 689 15. Espinet C, de la Torre MA, Aldea M, Herrero E. An efficient method to isolate yeast  
690 genes causing overexpression-mediated growth arrest. *Yeast* **11**, 25-32 (1995).  
691
- 692 16. Akada R, Yamamoto J, Yamashita I. Screening and identification of yeast sequences that  
693 cause growth inhibition when overexpressed. *Mol Gen Genet* **254**, 267-274 (1997).  
694
- 695 17. Legrand M, Jaitly P, Feri A, d'Enfert C, Sanyal K. *Candida albicans*: An Emerging Yeast  
696 Model to Study Eukaryotic Genome Plasticity. *Trends Genet* **35**, 292-307 (2019).  
697
- 698 18. Brown GD, Denning DW, Gow NA, Levitz SM, Netea MG, White TC. Hidden killers:  
699 human fungal infections. *Sci Transl Med* **4**, 165rv113 (2012).  
700
- 701 19. Friedman DZP, Schwartz IS. Emerging Fungal Infections: New Patients, New Patterns,  
702 and New Pathogens. *J Fungi (Basel)* **5**, (2019).  
703
- 704 20. Selmecki A, Forche A, Berman J. Genomic plasticity of the human fungal pathogen  
705 *Candida albicans*. *Eukaryot Cell* **9**, 991-1008 (2010).  
706
- 707 21. Forche A, Alby K, Schaefer D, Johnson AD, Berman J, Bennett RJ. The parasexual cycle  
708 in *Candida albicans* provides an alternative pathway to meiosis for the formation of  
709 recombinant strains. *PLoS Biol* **6**, e110 (2008).  
710
- 711 22. Feri A, *et al.* Analysis of Repair Mechanisms following an Induced Double-Strand Break  
712 Uncovers Recessive Deleterious Alleles in the *Candida albicans* Diploid Genome. *mBio*  
713 **7**, (2016).  
714
- 715 23. Selmecki A, Gerami-Nejad M, Paulson C, Forche A, Berman J. An isochromosome  
716 confers drug resistance in vivo by amplification of two genes, ERG11 and TAC1. *Mol*  
717 *Microbiol* **68**, 624-641 (2008).  
718
- 719 24. Dunkel N, Blass J, Rogers PD, Morschhauser J. Mutations in the multi-drug resistance  
720 regulator MRR1, followed by loss of heterozygosity, are the main cause of MDR1  
721 overexpression in fluconazole-resistant *Candida albicans* strains. *Mol Microbiol* **69**, 827-  
722 840 (2008).  
723
- 724 25. Selmecki AM, Dulmage K, Cowen LE, Anderson JB, Berman J. Acquisition of  
725 aneuploidy provides increased fitness during the evolution of antifungal drug resistance.  
726 *PLoS Genet* **5**, e1000705 (2009).  
727
- 728 26. Ford CB, *et al.* The evolution of drug resistance in clinical isolates of *Candida albicans*.  
729 *Elife* **4**, e00662 (2015).  
730
- 731 27. Selmecki A, Forche A, Berman J. Aneuploidy and isochromosome formation in drug-  
732 resistant *Candida albicans*. *Science* **313**, 367-370 (2006).  
733
- 734 28. Coste A, *et al.* A mutation in Tac1p, a transcription factor regulating CDR1 and CDR2, is  
735 coupled with loss of heterozygosity at chromosome 5 to mediate antifungal resistance in  
736 *Candida albicans*. *Genetics* **172**, 2139-2156 (2006).  
737

- 738 29. Forche A, *et al.* Rapid Phenotypic and Genotypic Diversification After Exposure to the  
739 Oral Host Niche in *Candida albicans*. *Genetics* **209**, 725-741 (2018).  
740
- 741 30. Tso GHW, *et al.* Experimental evolution of a fungal pathogen into a gut symbiont. *Science*  
742 **362**, 589-595 (2018).  
743
- 744 31. Forche A, Magee PT, Selmecki A, Berman J, May G. Evolution in *Candida albicans*  
745 populations during a single passage through a mouse host. *Genetics* **182**, 799-811 (2009).  
746
- 747 32. Bennett RJ, Forche A, Berman J. Rapid mechanisms for generating genome diversity:  
748 whole ploidy shifts, aneuploidy, and loss of heterozygosity. *Cold Spring Harb Perspect*  
749 *Med* **4**, (2014).  
750
- 751 33. Sanyal K, Carbon J. The CENP-A homolog CaCse4p in the pathogenic yeast *Candida*  
752 *albicans* is a centromere protein essential for chromosome transmission. *Proc Natl Acad*  
753 *Sci U S A* **99**, 12969-12974 (2002).  
754
- 755 34. Sanyal K, Baum M, Carbon J. Centromeric DNA sequences in the pathogenic yeast  
756 *Candida albicans* are all different and unique. *Proc Natl Acad Sci U S A* **101**, 11374-  
757 11379 (2004).  
758
- 759 35. Guin K, Sreekumar L, Sanyal K. Implications of the Evolutionary Trajectory of  
760 Centromeres in the Fungal Kingdom. *Annu Rev Microbiol* **74**, 835-853 (2020).  
761
- 762 36. Musacchio A, Desai A. A Molecular View of Kinetochores Assembly and Function.  
763 *Biology (Basel)* **6**, (2017).  
764
- 765 37. Varshney N, Sanyal K. Nuclear migration in budding yeasts: position before division.  
766 *Curr Genet* **65**, 1341-1346 (2019).  
767
- 768 38. Gonzalez-Novo A, *et al.* Dbf2 is essential for cytokinesis and correct mitotic spindle  
769 formation in *Candida albicans*. *Mol Microbiol* **72**, 1364-1378 (2009).  
770
- 771 39. Milne SW, *et al.* Role of *Candida albicans* Tem1 in mitotic exit and cytokinesis. *Fungal*  
772 *Genet Biol* **69**, 84-95 (2014).  
773
- 774 40. Bates S. *Candida albicans* Cdc15 is essential for mitotic exit and cytokinesis. *Sci Rep* **8**,  
775 8899 (2018).  
776
- 777 41. Thakur J, Sanyal K. The essentiality of the fungus-specific Dam1 complex is correlated  
778 with a one-kinetochore-one-microtubule interaction present throughout the cell cycle,  
779 independent of the nature of a centromere. *Eukaryot Cell* **10**, 1295-1305 (2011).  
780
- 781 42. Roy B, Burrack LS, Lone MA, Berman J, Sanyal K. CaMtw1, a member of the  
782 evolutionarily conserved Mis12 kinetochore protein family, is required for efficient inner  
783 kinetochore assembly in the pathogenic yeast *Candida albicans*. *Mol Microbiol* **80**, 14-32  
784 (2011).  
785

- 786 43. Legrand M, Chan CL, Jauert PA, Kirkpatrick DT. Role of DNA mismatch repair and  
787 double-strand break repair in genome stability and antifungal drug resistance in *Candida*  
788 *albicans*. *Eukaryot Cell* **6**, 2194-2205 (2007).
- 789  
790 44. Legrand M, Chan CL, Jauert PA, Kirkpatrick DT. The contribution of the S-phase  
791 checkpoint genes MEC1 and SGS1 to genome stability maintenance in *Candida albicans*.  
792 *Fungal Genet Biol* **48**, 823-830 (2011).
- 793  
794 45. Loll-Krippelber R, *et al.* A study of the DNA damage checkpoint in *Candida albicans*:  
795 uncoupling of the functions of Rad53 in DNA repair, cell cycle regulation and genotoxic  
796 stress-induced polarized growth. *Mol Microbiol* **91**, 452-471 (2014).
- 797  
798 46. Loll-Krippelber R, *et al.* A FACS-optimized screen identifies regulators of genome  
799 stability in *Candida albicans*. *Eukaryot Cell* **14**, 311-322 (2015).
- 800  
801 47. Chauvel M, *et al.* A versatile overexpression strategy in the pathogenic yeast *Candida*  
802 *albicans*: identification of regulators of morphogenesis and fitness. *PLoS One* **7**, e45912  
803 (2012).
- 804  
805 48. Bachewich C, Nantel A, Whiteway M. Cell cycle arrest during S or M phase generates  
806 polarized growth via distinct signals in *Candida albicans*. *Mol Microbiol* **57**, 942-959  
807 (2005).
- 808  
809 49. Bensen ES, Clemente-Blanco A, Finley KR, Correa-Bordes J, Berman J. The mitotic  
810 cyclins Clb2p and Clb4p affect morphogenesis in *Candida albicans*. *Mol Biol Cell* **16**,  
811 3387-3400 (2005).
- 812  
813 50. Thakur J, Sanyal K. A coordinated interdependent protein circuitry stabilizes the  
814 kinetochore ensemble to protect CENP-A in the human pathogenic yeast *Candida*  
815 *albicans*. *PLoS Genet* **8**, e1002661 (2012).
- 816  
817 51. Kitamura E, Tanaka K, Kitamura Y, Tanaka TU. Kinetochore microtubule interaction  
818 during S phase in *Saccharomyces cerevisiae*. *Genes Dev* **21**, 3319-3330 (2007).
- 819  
820 52. Jin QW, Fuchs J, Loidl J. Centromere clustering is a major determinant of yeast interphase  
821 nuclear organization. *J Cell Sci* **113** ( Pt 11), 1903-1912 (2000).
- 822  
823 53. Lin TC, Neuner A, Schiebel E. Targeting of gamma-tubulin complexes to microtubule  
824 organizing centers: conservation and divergence. *Trends Cell Biol* **25**, 296-307 (2015).
- 825  
826 54. Lin TC, *et al.* MOZART1 and gamma-tubulin complex receptors are both required to turn  
827 gamma-TuSC into an active microtubule nucleation template. *J Cell Biol* **215**, 823-840  
828 (2016).
- 829  
830 55. Musacchio A, Salmon ED. The spindle-assembly checkpoint in space and time. *Nat Rev*  
831 *Mol Cell Biol* **8**, 379-393 (2007).
- 832  
833 56. Kops G, Snel B, Tromer EC. Evolutionary Dynamics of the Spindle Assembly Checkpoint  
834 in Eukaryotes. *Curr Biol* **30**, R589-R602 (2020).
- 835

- 836 57. Caydasi AK, Pereira G. SPOC alert--when chromosomes get the wrong direction. *Exp*  
837 *Cell Res* **318**, 1421-1427 (2012).  
838
- 839 58. Scarfone I, Piatti S. Coupling spindle position with mitotic exit in budding yeast: The  
840 multifaceted role of the small GTPase Tem1. *Small GTPases* **6**, 196-201 (2015).  
841
- 842 59. Care RS, Trevethick J, Binley KM, Sudbery PE. The MET3 promoter: a new tool for  
843 *Candida albicans* molecular genetics. *Mol Microbiol* **34**, 792-798 (1999).  
844
- 845 60. Shivaraju M, Unruh JR, Slaughter BD, Mattingly M, Berman J, Gerton JL. Cell-cycle-  
846 coupled structural oscillation of centromeric nucleosomes in yeast. *Cell* **150**, 304-316  
847 (2012).  
848
- 849 61. Sreekumar L, *et al.* Orc4 spatiotemporally stabilizes centromeric chromatin. *Genome Res*  
850 **31**, 607-621 (2021).  
851
- 852 62. Liu HY, Toyn JH, Chiang YC, Draper MP, Johnston LH, Denis CL. DBF2, a cell cycle-  
853 regulated protein kinase, is physically and functionally associated with the CCR4  
854 transcriptional regulatory complex. *EMBO J* **16**, 5289-5298 (1997).  
855
- 856 63. Surana U, Amon A, Dowzer C, McGrew J, Byers B, Nasmyth K. Destruction of the  
857 CDC28/CLB mitotic kinase is not required for the metaphase to anaphase transition in  
858 budding yeast. *EMBO J* **12**, 1969-1978 (1993).  
859
- 860 64. Hotz M, Barral Y. The Mitotic Exit Network: new turns on old pathways. *Trends Cell Biol*  
861 **24**, 145-152 (2014).  
862
- 863 65. Atir-Lande A, Gildor T, Kornitzer D. Role for the SCFCDC4 ubiquitin ligase in *Candida*  
864 *albicans* morphogenesis. *Mol Biol Cell* **16**, 2772-2785 (2005).  
865
- 866 66. Shirayama M, Matsui Y, Toh EA. The yeast TEM1 gene, which encodes a GTP-binding  
867 protein, is involved in termination of M phase. *Mol Cell Biol* **14**, 7476-7482 (1994).  
868
- 869 67. Valerio-Santiago M, Monje-Casas F. Tem1 localization to the spindle pole bodies is  
870 essential for mitotic exit and impairs spindle checkpoint function. *J Cell Biol* **192**, 599-614  
871 (2011).  
872
- 873 68. Lee SE, Frenz LM, Wells NJ, Johnson AL, Johnston LH. Order of function of the  
874 budding-yeast mitotic exit-network proteins Tem1, Cdc15, Mob1, Dbf2, and Cdc5. *Curr*  
875 *Biol* **11**, 784-788 (2001).  
876
- 877 69. Jackson AP, *et al.* Comparative genomics of the fungal pathogens *Candida dubliniensis*  
878 and *Candida albicans*. *Genome Res* **19**, 2231-2244 (2009).  
879
- 880 70. Padmanabhan S, Thakur J, Siddharthan R, Sanyal K. Rapid evolution of Cse4p-rich  
881 centromeric DNA sequences in closely related pathogenic yeasts, *Candida albicans* and  
882 *Candida dubliniensis*. *Proc Natl Acad Sci U S A* **105**, 19797-19802 (2008).  
883
- 884 71. Chatterjee G, *et al.* Repeat-Associated Fission Yeast-Like Regional Centromeres in the  
885 Ascomycetous Budding Yeast *Candida tropicalis*. *PLoS Genet* **12**, e1005839 (2016).

886  
887  
888  
889  
890  
891  
892  
893  
894  
895  
896  
897  
898  
899  
900  
901  
902  
903  
904  
905  
906  
907  
908  
909  
910  
911  
912  
913  
914  
915  
916  
917  
918  
919  
920  
921  
922  
923  
924  
925  
926  
927  
928  
929  
930  
931  
932  
933  
934  
935

72. Bijlani S, Thevandavakkam MA, Tsai HJ, Berman J. Autonomously Replicating Linear Plasmids That Facilitate the Analysis of Replication Origin Function in *Candida albicans*. *mSphere* **4**, (2019).
73. Pellman D, Bagget M, Tu YH, Fink GR, Tu H. Two microtubule-associated proteins required for anaphase spindle movement in *Saccharomyces cerevisiae*. *J Cell Biol* **130**, 1373-1385 (1995).
74. Schuyler SC, Liu JY, Pellman D. The molecular function of Ase1p: evidence for a MAP-dependent midzone-specific spindle matrix. Microtubule-associated proteins. *J Cell Biol* **160**, 517-528 (2003).
75. Liu H, Liang F, Jin F, Wang Y. The coordination of centromere replication, spindle formation, and kinetochore-microtubule interaction in budding yeast. *PLoS Genet* **4**, e1000262 (2008).
76. Wang Y, Hu F, Elledge SJ. The Bfa1/Bub2 GAP complex comprises a universal checkpoint required to prevent mitotic exit. *Curr Biol* **10**, 1379-1382 (2000).
77. Ro HS, Song S, Lee KS. Bfa1 can regulate Tem1 function independently of Bub2 in the mitotic exit network of *Saccharomyces cerevisiae*. *Proc Natl Acad Sci U S A* **99**, 5436-5441 (2002).
78. Ofir A, Kornitzer D. *Candida albicans* cyclin Clb4 carries S-phase cyclin activity. *Eukaryot Cell* **9**, 1311-1319 (2010).
79. Schwob E, Nasmyth K. CLB5 and CLB6, a new pair of B cyclins involved in DNA replication in *Saccharomyces cerevisiae*. *Genes Dev* **7**, 1160-1175 (1993).
80. Hibbel A, et al. Kinesin Kip2 enhances microtubule growth in vitro through length-dependent feedback on polymerization and catastrophe. *Elife* **4**, (2015).
81. Augustine B, Chin CF, Yeong FM. Role of Kip2 during early mitosis - impact on spindle pole body separation and chromosome capture. *J Cell Sci* **131**, (2018).
82. Riera A, Barbon M, Noguchi Y, Reuter LM, Schneider S, Speck C. From structure to mechanism-understanding initiation of DNA replication. *Genes Dev* **31**, 1073-1088 (2017).
83. Labib K, Tercero JA, Diffley JF. Uninterrupted MCM2-7 function required for DNA replication fork progression. *Science* **288**, 1643-1647 (2000).
84. Ren B, et al. MCM7 amplification and overexpression are associated with prostate cancer progression. *Oncogene* **25**, 1090-1098 (2006).
85. Toyokawa G, et al. Minichromosome Maintenance Protein 7 is a potential therapeutic target in human cancer and a novel prognostic marker of non-small cell lung cancer. *Mol Cancer* **10**, 65 (2011).

- 936 86. Qiu YT, Wang WJ, Zhang B, Mei LL, Shi ZZ. MCM7 amplification and overexpression  
937 promote cell proliferation, colony formation and migration in esophageal squamous cell  
938 carcinoma by activating the AKT1/mTOR signaling pathway. *Oncol Rep* **37**, 3590-3596  
939 (2017).  
940
- 941 87. Weinert TA, Hartwell LH. The RAD9 gene controls the cell cycle response to DNA  
942 damage in *Saccharomyces cerevisiae*. *Science* **241**, 317-322 (1988).  
943
- 944 88. Waterman DP, Haber JE, Smolka MB. Checkpoint Responses to DNA Double-Strand  
945 Breaks. *Annu Rev Biochem* **89**, 103-133 (2020).  
946
- 947 89. Sridhar S, Hori T, Nakagawa R, Fukagawa T, Sanyal K. Bridgin connects the outer  
948 kinetochore to centromeric chromatin. *Nat Commun* **12**, 146 (2021).  
949
- 950 90. Zhang Y, *et al.* USP44 regulates centrosome positioning to prevent aneuploidy and  
951 suppress tumorigenesis. *J Clin Invest* **122**, 4362-4374 (2012).  
952
- 953 91. Silkworth WT, Nardi IK, Paul R, Mogilner A, Cimini D. Timing of centrosome separation  
954 is important for accurate chromosome segregation. *Mol Biol Cell* **23**, 401-411 (2012).  
955
- 956 92. Nam HJ, Naylor RM, van Deursen JM. Centrosome dynamics as a source of chromosomal  
957 instability. *Trends Cell Biol* **25**, 65-73 (2015).  
958
- 959 93. Clemente-Blanco A, *et al.* The Cdc14p phosphatase affects late cell-cycle events and  
960 morphogenesis in *Candida albicans*. *J Cell Sci* **119**, 1130-1143 (2006).  
961
- 962 94. Kaneva IN, Sudbery IM, Dickman MJ, Sudbery PE. Proteins that physically interact with  
963 the phosphatase Cdc14 in *Candida albicans* have diverse roles in the cell cycle. *Sci Rep* **9**,  
964 6258 (2019).  
965
- 966 95. Segal ES, *et al.* Gene Essentiality Analyzed by In Vivo Transposon Mutagenesis and  
967 Machine Learning in a Stable Haploid Isolate of *Candida albicans*. *mBio* **9**, (2018).  
968
- 969 96. Chung CT, Niemela SL, Miller RH. One-step preparation of competent *Escherichia coli*:  
970 transformation and storage of bacterial cells in the same solution. *Proc Natl Acad Sci U S*  
971 *A* **86**, 2172-2175 (1989).  
972
- 973 97. Potter SC, Luciani A, Eddy SR, Park Y, Lopez R, Finn RD. HMMER web server: 2018  
974 update. *Nucleic Acids Res* **46**, W200-W204 (2018).  
975
- 976 98. Luca FC, Mody M, Kurischko C, Roof DM, Giddings TH, Winey M. *Saccharomyces*  
977 *cerevisiae* Mob1p is required for cytokinesis and mitotic exit. *Mol Cell Biol* **21**, 6972-  
978 6983 (2001).  
979
- 980 99. Tamborrini D, Juanes MA, Ibanes S, Rancati G, Piatti S. Recruitment of the mitotic exit  
981 network to yeast centrosomes couples septin displacement to actomyosin constriction. *Nat*  
982 *Commun* **9**, 4308 (2018).  
983
- 984 100. Sopko R, *et al.* Mapping pathways and phenotypes by systematic gene overexpression.  
985 *Mol Cell* **21**, 319-330 (2006).

986  
987 101. Li R. Bifurcation of the mitotic checkpoint pathway in budding yeast. *Proc Natl Acad Sci*  
988 *USA* **96**, 4989-4994 (1999).

## 991 **Acknowledgments**

992  
993 We thank members of the Sanyal and d'Enfert laboratories for their valuable suggestions and  
994 constructive criticism. We thank the Munro group at University of Aberdeen and Mazel group at  
995 Institut Pasteur for their contribution to the establishment of overexpression plasmids that were  
996 used in this study, a work that will be reported elsewhere. We thank Dr. Arshad Desai for critical  
997 reading of the manuscript. We thank N. Varshney for constructing the plasmid pCse4-TAP-Leu.  
998 We thank L. Sreekumar for constructing pTub4-GFP-His cassette. Special thanks to K. Guin for  
999 sharing the raw files to generate the phylogenetic tree. We thank V. Sood and A. Das for  
1000 generating the plasmid pCdCsa6-GFP-ARS2. We thank A.S. Amrutha for generating the strains  
1001 CaPJ300 and CaPJ301. We acknowledge N. Nala at the flow cytometry facility, JNCASR, for  
1002 assisting flow cytometry and cell sorting experiments. The establishment of overexpression  
1003 plasmids was supported by the Wellcome Trust [088858/Z/09/Z to CD]. This work was supported  
1004 by a grant from the Indo French Centre for the promotion of Advanced Research (CEFIPRA,  
1005 Project no. 5703-2). CEFIPRA also aided in the travel of PJ, KS and CD between the Sanyal and  
1006 d'Enfert laboratories. PJ acknowledges intramural funding from JNCASR. AD and TP were  
1007 supported by the CEFIPRA grant. K.S. acknowledges the financial support of JC Bose National  
1008 Fellowship (Science and Engineering Research Board, Govt. of India, JCB/2020/000021) and  
1009 intramural funding from JNCASR.

## 1011 **Funding**

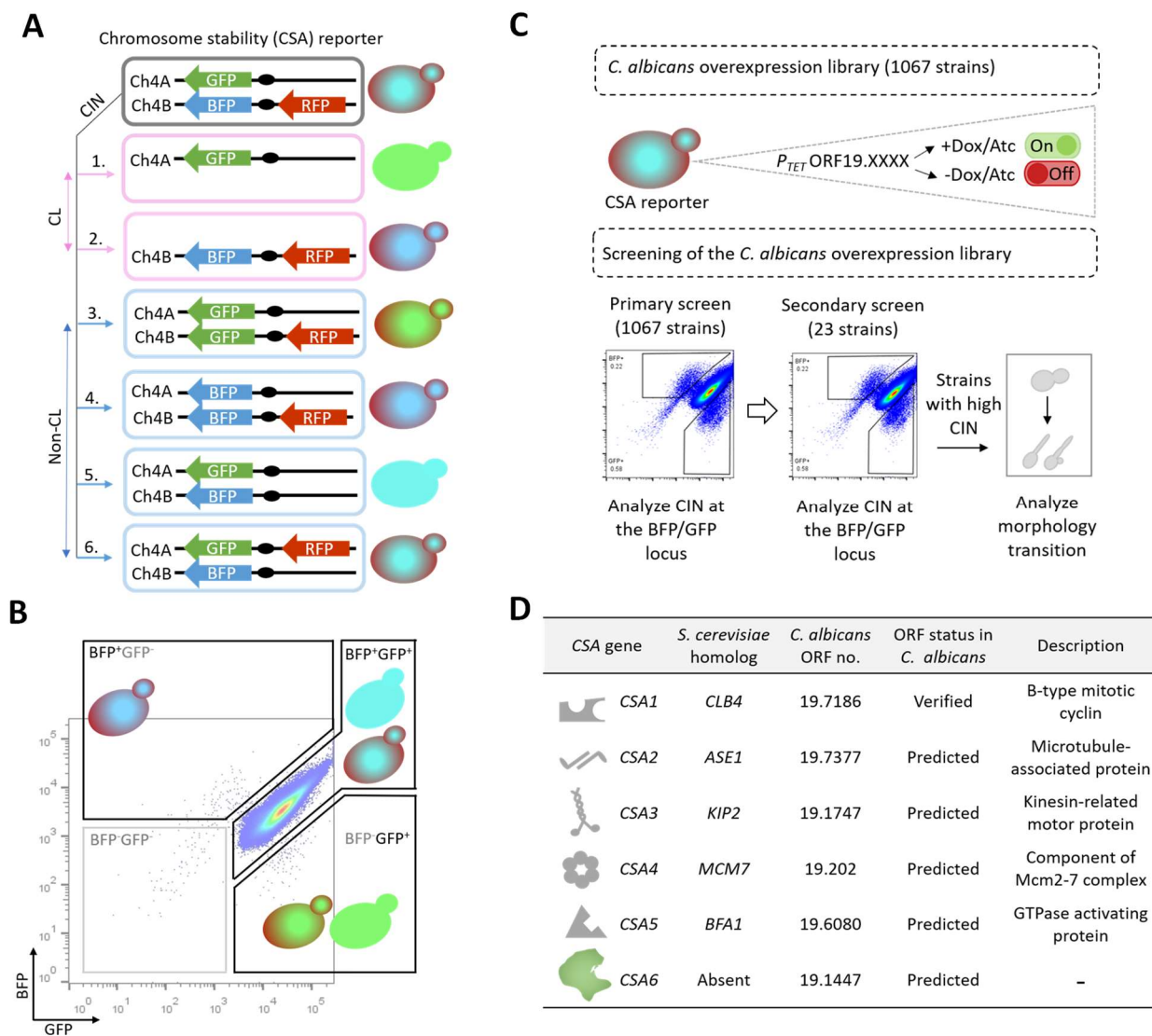
1012  
1013 Indo French Centre for the promotion of Advanced Research (CEFIPRA, Project no. 5703-2).  
1014 Jawaharlal Nehru Centre for Advanced Scientific Research.  
1015 JC Bose National Fellowship (Science and Engineering Research Board, Govt. of India,  
1016 JCB/2020/000021).  
1017 The Wellcome Trust (088858/Z/09/Z).  
1018 Institut Pasteur.  
1019 Institut national de la recherche pour l'agriculture, l'alimentation et l'environnement (INRAE).

1021 **Author contributions:**  
1022 Conceptualization: KS, CD, PJ, ML  
1023 Methodology: ML, PJ, AD, TP, MC  
1024 Investigation: PJ, AD, TP, ML  
1025 Supervision: KS, CD, ML  
1026 Writing—original draft: PJ, KS  
1027 Writing—review & editing: PJ, KS, CD, ML

1028  
1029 **Competing interests:** The authors declare no competing interests.

1030  
1031 **Data and materials availability:** All data are available in the main text or supplementary  
1032 materials.

1033  
1034  
1035  
1036  
1037  
1038  
1039  
1040  
1041  
1042  
1043  
1044  
1045  
1046  
1047  
1048  
1049  
1050  
1051  
1052  
1053  
1054



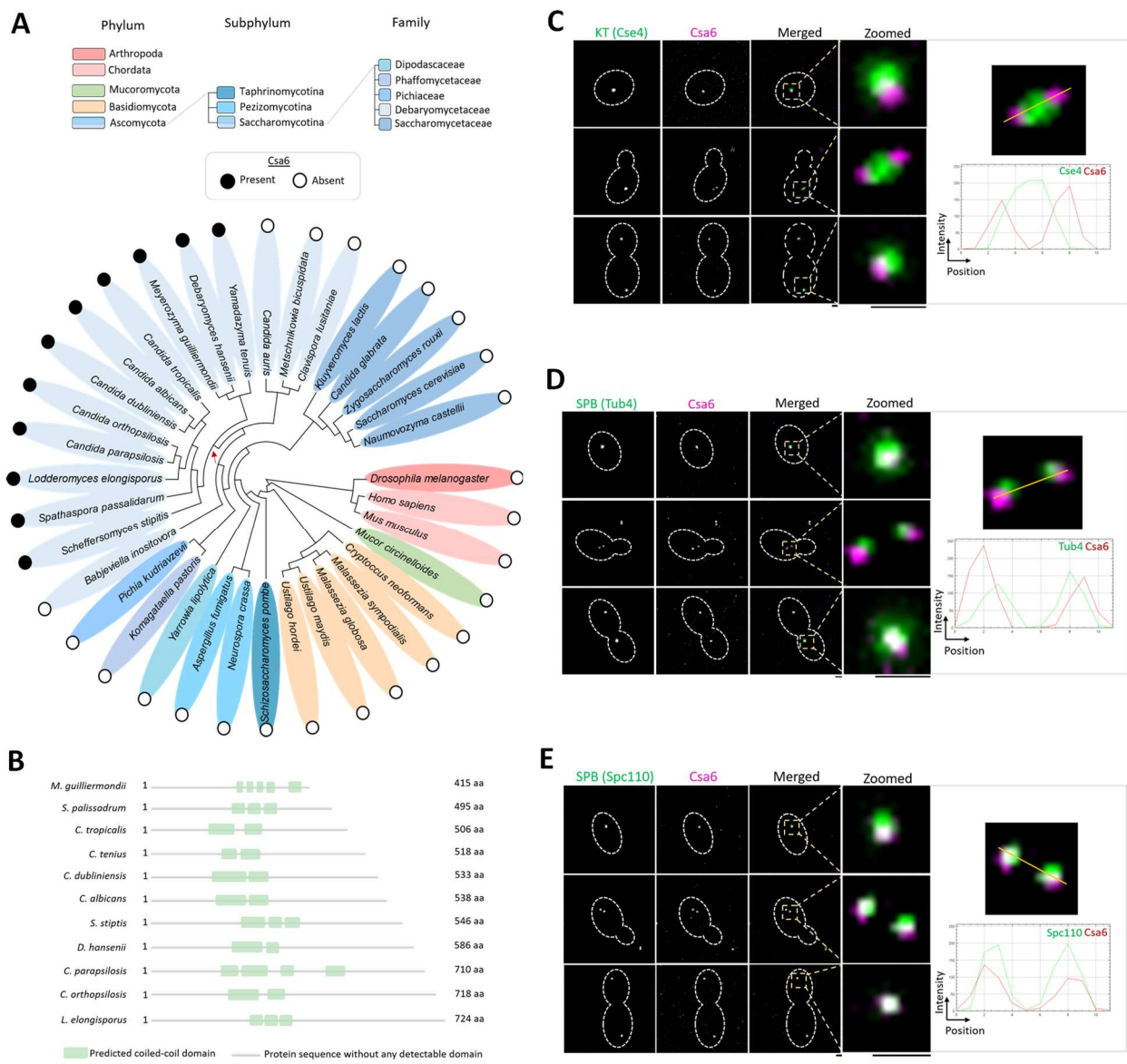
1056

1057

1058 **Fig. 1. A medium-throughput protein overexpression screen identifies a set of CSA genes in**  
 1059 ***C. albicans*. (A)** Possible outcomes of CIN at the BFP/GFP and RFP loci. 1-4, CIN at the BFP or  
 1060 GFP locus, because of either chromosome loss (CL) or non-CL events such as break-induced  
 1061 replication, gene conversion, chromosome truncation or mitotic crossing over, will lead to the  
 1062 expression of either GFP or BFP expressing genes. CIN due to CL can be specifically identified  
 1063 by the concomitant loss of BFP and RFP, as shown in 1. 5 and 6, cells undergoing non-CL events  
 1064 at the RFP locus will continue to express BFP and GFP. **(B)** Flow cytometric analysis of the  
 1065 BFP/GFP density profile of empty vector (EV) (CaPJ150) containing BFP, GFP and RFP genes.  
 1066 Majority of the cells are positive for both BFP and GFP (BFP<sup>+</sup>GFP<sup>+</sup>). A minor fraction of the  
 1067 population had lost either one of the markers (BFP<sup>+</sup>GFP<sup>-</sup> or BFP<sup>-</sup>GFP<sup>+</sup>) or both the markers (BFP<sup>-</sup>

1068 GFP<sup>+</sup>), indicating spontaneous instability of this locus <sup>46</sup>. Approximately 1 million events are  
1069 displayed. **(C)** Pictorial representation of the screening strategy employed for identifying *CSA*  
1070 genes in *C. albicans*. Briefly, a library of *C. albicans* overexpression strains (1067), each carrying  
1071 a unique ORF under the tetracycline-inducible promoter, P<sub>TET</sub>, was generated using the *CSA*  
1072 reporter (CEC5201) as the parent strain. The library was then analyzed by primary and secondary  
1073 screening methods to identify *CSA* genes. In the primary screen, CIN frequency at the BFP/GFP  
1074 locus in the individual 1067 overexpression strains was determined using flow cytometry.  
1075 Overexpression strains exhibiting increased CIN (23 out of 1067) were taken forward for  
1076 secondary screening. The secondary screen involved revalidation of the primary hits for increased  
1077 CIN at the BFP/GFP locus by flow cytometry. Strains which reproduced the increased CIN  
1078 phenotype were further examined for yeast to filamentous transition by microscopy. **(D)** A brief  
1079 overview of the *CSA* genes identified from the overexpression screen (6 out of 1067). Functional  
1080 annotation of genes is based on the information available either in *Candida Genome Database*  
1081 ([www.candidagenome.org](http://www.candidagenome.org)) or in *Saccharomyces Genome Database* ([www.yeastgenome.org](http://www.yeastgenome.org)) on  
1082 August 1, 2021.

1083  
1084  
1085  
1086  
1087  
1088  
1089  
1090  
1091  
1092  
1093  
1094  
1095  
1096  
1097  
1098  
1099  
1100  
1101



1104  
 1105  
 1106 **Fig. 2. Csa6 has a selective existence across fungal phylogeny and is constitutively localized**  
 1107 **to the SPBs in *C. albicans*.** (A) Phylogenetic tree showing the conservation of Csa6 across the  
 1108 mentioned species. The presence (filled circles) or absence (empty circles) of Csa6 in every  
 1109 species is marked. Each taxonomic rank is color-coded. The species mentioned under the family  
 1110 Debaryomycetaceae belong to the CUG-Ser clade in which the CUG codon is often translated as  
 1111 serine instead of leucine. The red arrow points to the CUG-Ser clade lineage that acquired Csa6.  
 1112 Searches for Csa6 homologs ( $E$  value  $\leq 10^{-2}$ ) were carried out either in the *Candida Genome*  
 1113 *Database* ([www.candidagenome.org](http://www.candidagenome.org)) or NCBI nonredundant protein database. (B) Schematic  
 1114 illustrating the protein domain architecture alignment of Csa6 in the indicated fungal species.

1115 Length of the protein is mentioned as amino acids (aa). Approximate positions of the predicted  
1116 coiled-coil domain, identified using HMMER <sup>97</sup> phmmer searches, is shown. **(C-E)** *Left*,  
1117 micrographs comparing the sub-cellular localization of Csa6 with KT (Cse4) and SPB (Tub4 and  
1118 Spc110) at various cell cycle stages. *Top*, Csa6-mCherry and Cse4-GFP (CaPJ119); *middle*, Csa6-  
1119 mCherry and Tub4-GFP (CaPJ120), and *bottom*, Csa6m-Cherry and Spc110-GFP (CaPJ121).  
1120 Scale bar, 1  $\mu$ m. *Right*, histogram plots showing the fluorescence intensity profile of Csa6-  
1121 mCherry with Cse4-GFP (*top*), Tub4-GFP (*middle*) and Spc110-GFP (*bottom*) across the  
1122 indicated lines.

1123

1124

1125

1126

1127

1128

1129

1130

1131

1132

1133

1134

1135

1136

1137

1138

1139

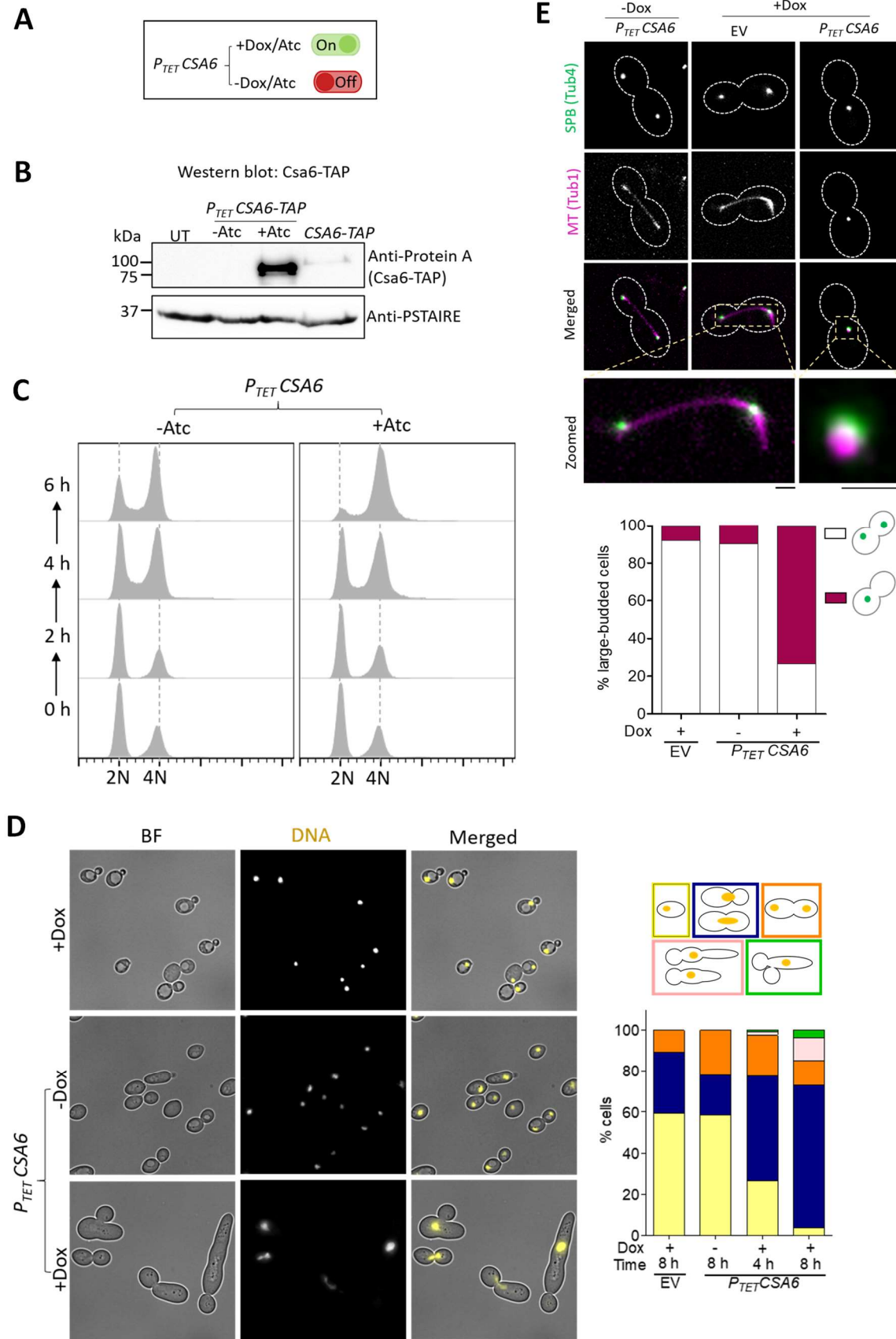
1140

1141

1142

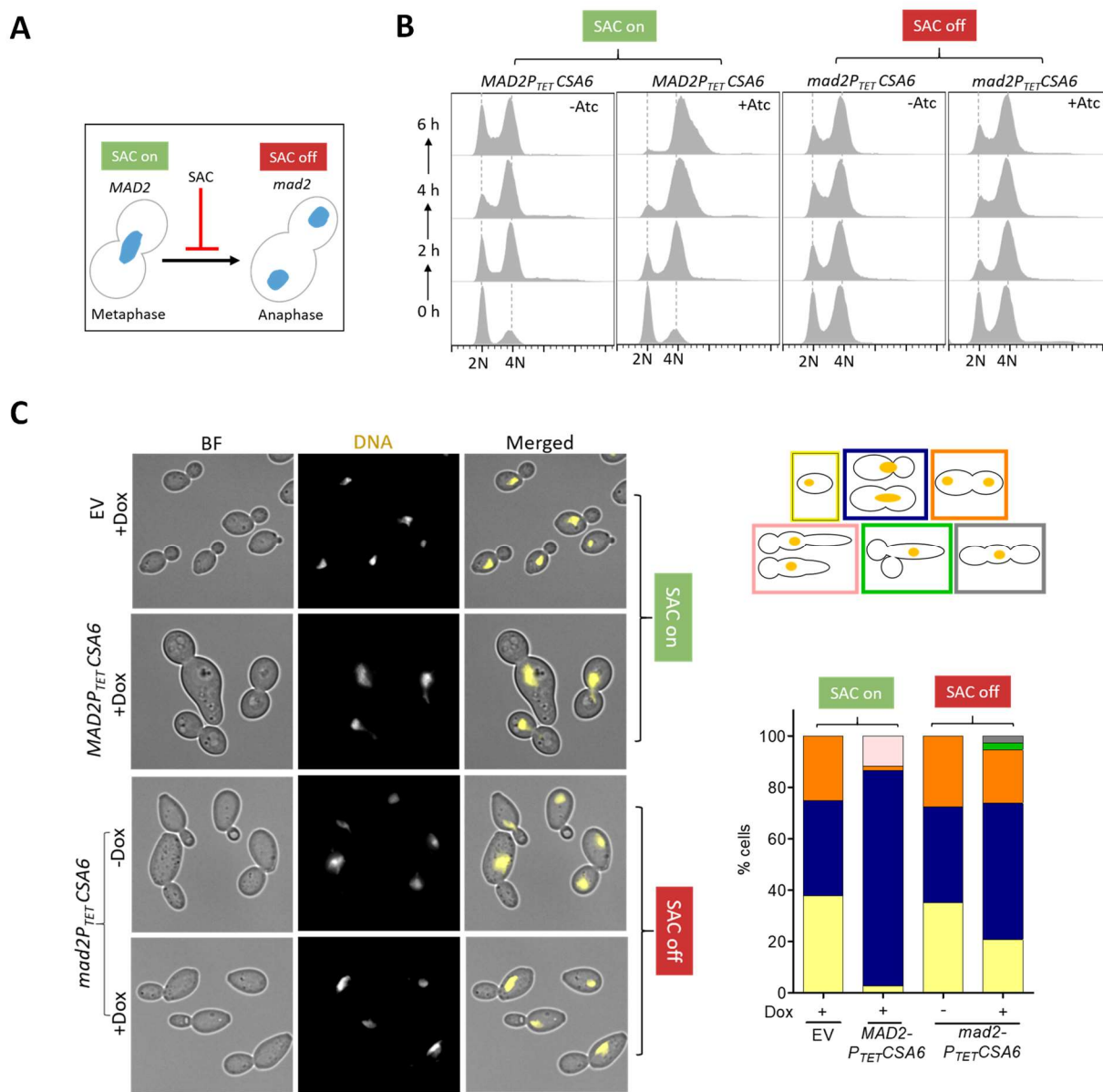
1143

1144



1148 **Fig. 3. Overexpression of Csa6 alters the morphology of the mitotic spindle and leads to**  
1149 **G2/M arrest in *C. albicans*.** (A) Atc/Dox-dependent functioning of the  $P_{TET}$  promoter system for  
1150 conditional overexpression of *CSA6*. (B) Western blot analysis using anti-Protein A antibodies  
1151 confirmed overexpression of *CSA6-TAP* from the  $P_{TET}$  promoter (CaPJ181), after 8 h induction in  
1152 presence of Atc (3  $\mu\text{g/ml}$ ), in comparison to the uninduced culture (-Atc) or *CSA6-TAP*  
1153 expression from its native promoter (CaPJ180);  $N=2$ . PSTAIRE was used as a loading control.  
1154 UT, untagged control (SN148). (C) Flow cytometric analysis of cell cycle displaying the cellular  
1155 DNA content of *CSA6<sup>OE</sup>* strain (CaPJ176) in presence or absence of Atc (3  $\mu\text{g/ml}$ ) at the  
1156 indicated time intervals;  $N=3$ . (D) *Left*, microscopic images of Hoechst-stained EV (CaPJ170)  
1157 and *CSA6<sup>OE</sup>* strain (CaPJ176) after 8 h of growth under indicated conditions of Dox (50  $\mu\text{g/ml}$ ).  
1158 BF, bright-field. Scale bar, 10  $\mu\text{m}$ . *Right*, quantitation of different cell types at the indicated time-  
1159 points;  $n \geq 100$  cells. (E) *Top*, representative micrographs of spindle morphology in the large-  
1160 budded cells of EV (CaPJ172) and *CSA6<sup>OE</sup>* strain (CaPJ178) after 8 h of growth under indicated  
1161 conditions of Dox (50  $\mu\text{g/ml}$ ). SPBs and MTs are marked by Tub4-GFP and Tub1-mCherry,  
1162 respectively. Scale bar, 1  $\mu\text{m}$ . *Bottom*, the proportion of the large-budded cells with indicated SPB  
1163 phenotypes;  $n \geq 100$  cells.

1164  
1165  
1166  
1167  
1168  
1169  
1170  
1171  
1172  
1173  
1174  
1175  
1176  
1177  
1178  
1179  
1180  
1181

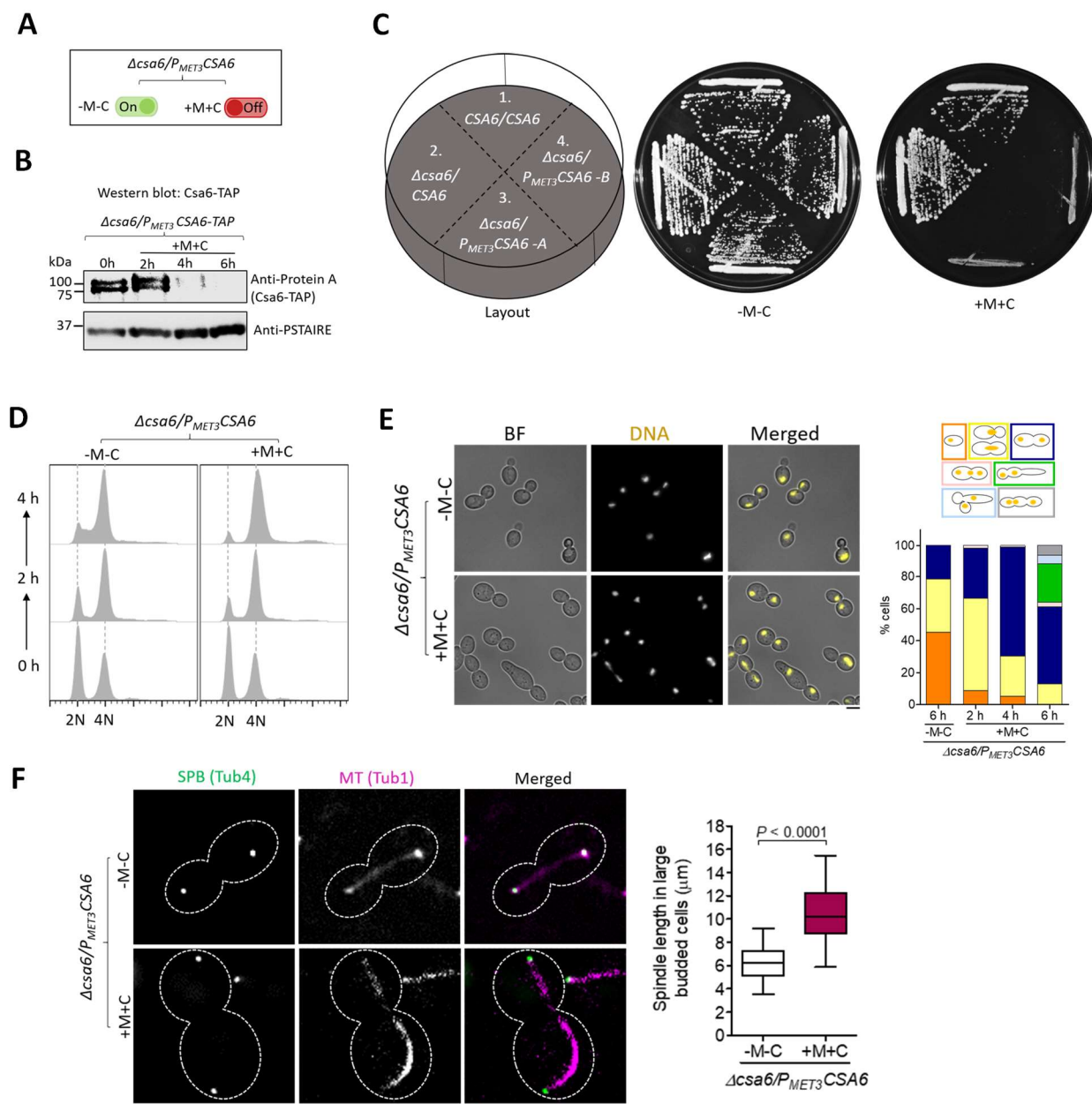


1183

1184

1185 **Fig. 4. The G2/M cell cycle arrest in the *CSA6*<sup>OE</sup> mutant is mediated by Mad2. (A) The**1186 **G2/M arrest posed by SAC in response to an improper chromosome-spindle attachment is**1187 **relieved in the absence of Mad2, allowing cells to transit from metaphase to anaphase. (B) Flow**1188 **cytometric DNA content analysis in CaPJ176 (*MAD2CSA6*<sup>OE</sup>) and CaPJ197 (*mad2CSA6*<sup>OE</sup>) at**1189 **the indicated times, in presence or absence of Atc (3  $\mu$ g/ml); *N*=3. (C) *Left*, microscopic images**1190 **of CaPJ170 (EV), CaPJ176 (*MAD2CSA6*<sup>OE</sup>) and CaPJ197 (*mad2CSA6*<sup>OE</sup>) following Hoechst**1191 **staining, after 8 h of growth under indicated conditions of Dox (50  $\mu$ g/ml). Scale bar, 10  $\mu$ m.**1192 ***Right*, quantitation of the indicated cell types; *n*  $\geq$ 100 cells.**

1193



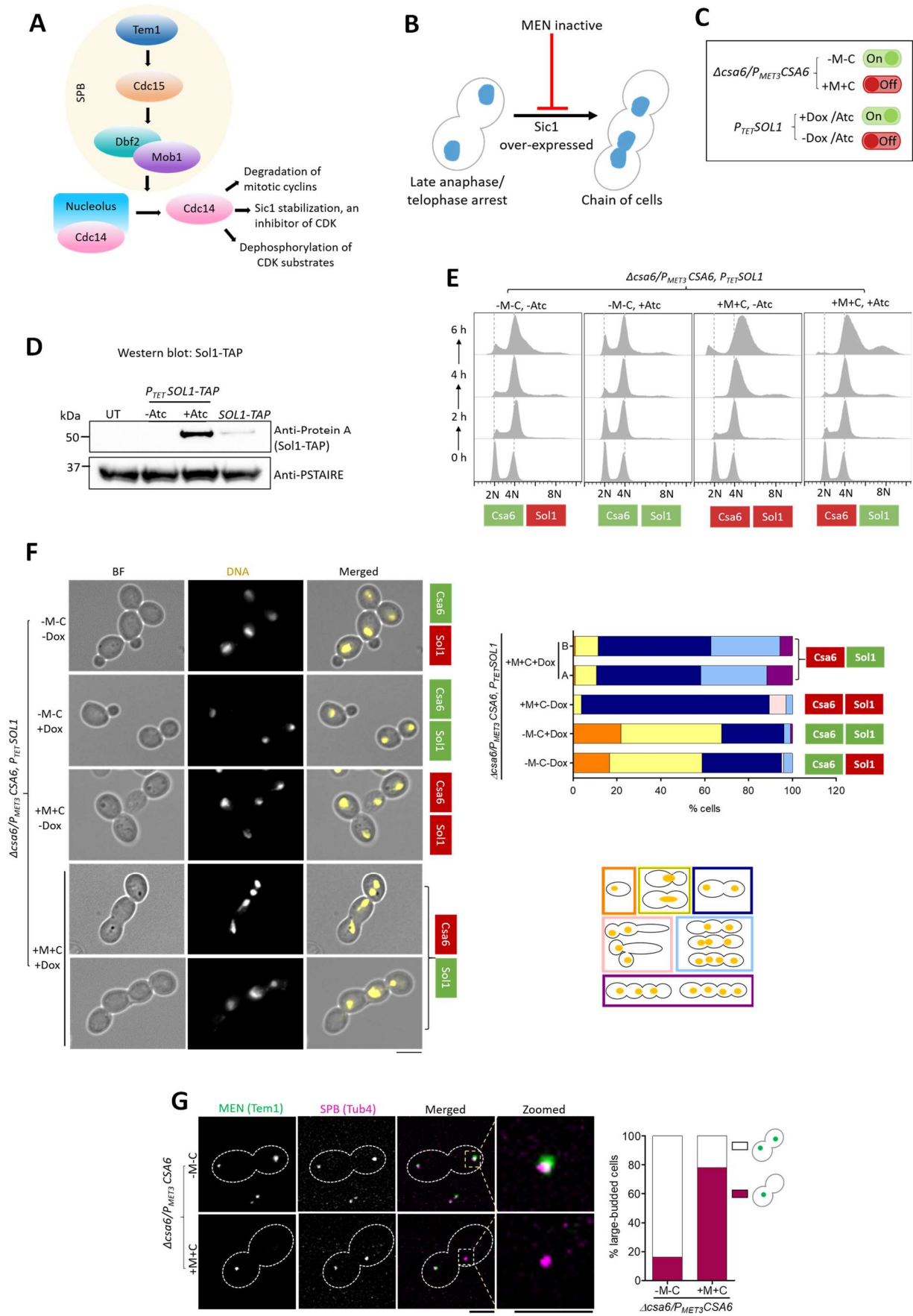
1195

1196

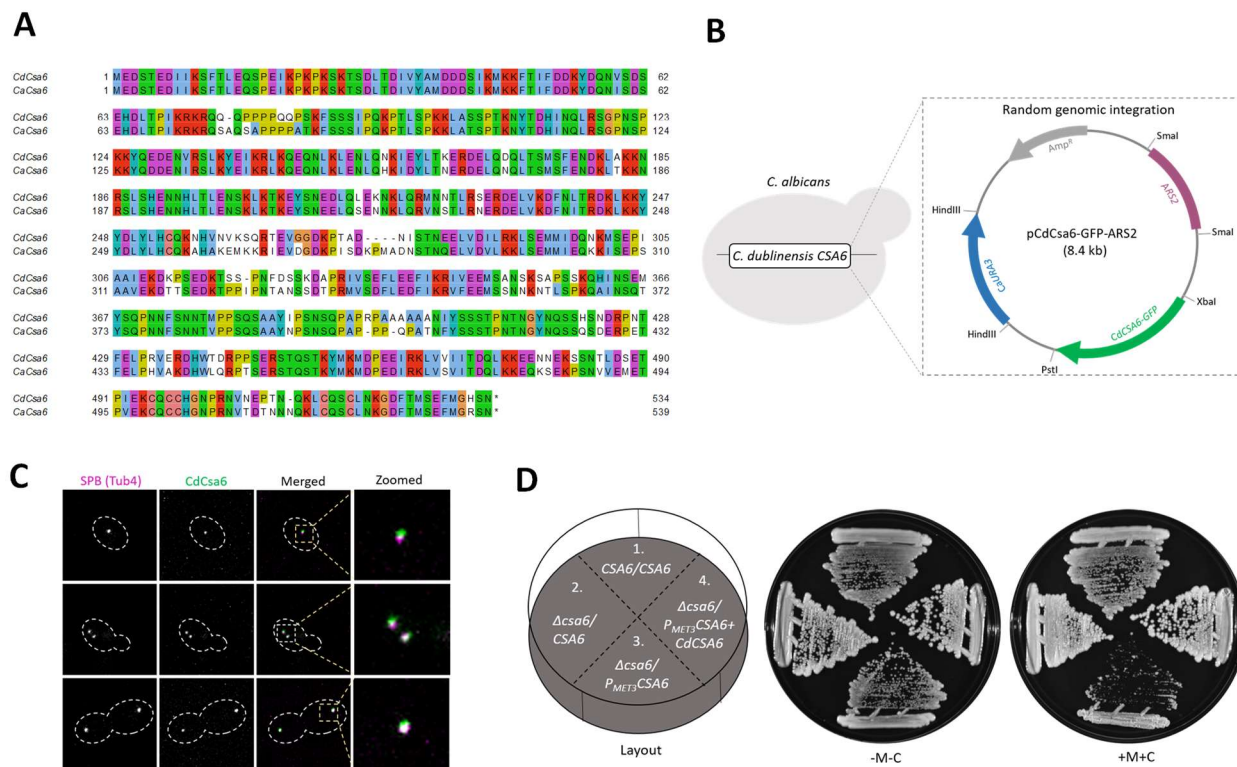
1197 **Fig. 5. Csa6 depletion causes late anaphase/telophase arrest with a hyper-extended mitotic**  
 1198 **spindle in *C. albicans*.** (A) The *MET3* promoter system for depleting cellular levels of Csa6. The  
 1199 *MET3* promoter can be conditionally repressed in presence of methionine (Met/M) and cysteine  
 1200 (Cys/C). (B) Western blot analysis using anti-Protein A antibodies revealed time dependent  
 1201 depletion of Csa6-TAP in *CSA6<sup>PSD</sup>* strain (CaPJ212), grown under repressive conditions (YPDU  
 1202 + 5 mM Met and 5 mM Cys) for indicated time interval; *N*=2. (C) Csa6 is essential for viability in  
 1203 *C. albicans*. Strains with indicated genotypes, (1) SN148, (2) CaPJ209, (3 and 4) CaPJ210 (two  
 1204 transformants) were streaked on agar plates with permissive (YPDU-Met-Cys) or repressive

1205 (YPDU + 5 mM Met and 5 mM Cys) media and incubated at 30°C for two days. **(D)** Cell cycle  
1206 analysis of CaPJ210 (*CSA6<sup>PSD</sup>*) by flow cytometry under permissive (YPDU-Met-Cys) and  
1207 repressive conditions (YPDU + 5 mM Met and 5 mM Cys) at the indicated time intervals;  $N=3$ .  
1208 **(E)** *Left*, microscopic images of Hoechst stained CaPJ210 (*CSA6<sup>PSD</sup>*) cells grown under  
1209 permissive (YPDU-Met-Cys) or repressive (YPDU + 5 mM Met and 5 mM Cys) conditions for 6  
1210 h. BF bright-field. Scale bar, 5  $\mu\text{m}$ . *Right*, quantitation of different cell types at the indicated time-  
1211 points;  $n \geq 100$  cells. **(F)** *Left*, micrograph showing Tub4-GFP and Tub1-mCherry (representing  
1212 mitotic spindle) in the large-budded cells of CaPJ211 (*CSA6<sup>PSD</sup>*) after 6 h of growth under  
1213 permissive (YPDU-Met-Cys) or repressive (YPDU + 5 mM Met and 5 mM Cys) conditions.  
1214 Scale bar, 3  $\mu\text{m}$ . *Right*, quantitation of the distance between the two SPBs, along the length of the  
1215 MT (representing spindle length), in large-budded cells of CaPJ211 (*CSA6<sup>PSD</sup>*) under permissive  
1216 ( $n=32$ ) or repressive ( $n=52$ ) conditions. Paired *t*-test, one-tailed, *P*-value shows a significant  
1217 difference.

1218  
1219  
1220  
1221  
1222  
1223  
1224  
1225  
1226  
1227  
1228  
1229  
1230  
1231  
1232  
1233  
1234  
1235  
1236  
1237  
1238



1241 **Fig. 6. Csa6 is required for mitotic exit in *C. albicans*.** (A) The MEN components in *S.*  
1242 *cerevisiae*. At SPB, Nud1 acts as a scaffold. The ultimate target of the MEN is to activate Cdc14  
1243 phosphatase, which remains entrapped in the nucleolus in an inactive state until anaphase. Cdc14  
1244 release brings about mitotic exit and cytokinesis by promoting degradation of mitotic cyclins,  
1245 inactivation of mitotic CDKs through Sic1 accumulation and dephosphorylation of the CDK  
1246 substrates<sup>64</sup>. (B) Inhibition of the MEN signaling prevents cells from exiting mitosis and arrests  
1247 them at late anaphase/telophase. Bypass of cell cycle arrest due to the inactive MEN, viz. by  
1248 overexpression of Sic1-a CDK inhibitor, results in the chain of cells with multiple nuclei<sup>98,99</sup>. (C)  
1249 A combination of two regulatable promoters,  $P_{TET}$  and  $P_{MET3}$ , was used to overexpress *C. albicans*  
1250 homolog of Sic1, called *SOLI* (Sic one-like), in Csa6-depleted cells. The resulting strain,  
1251 CaPJ215, can be conditionally induced for both *SOLI* overexpression upon Atc/Dox addition and  
1252 Csa6 depletion upon Met (M)/Cys (C) addition. (D) Protein A western blot analysis showed  
1253 increased levels of Sol1 (TAP-tagged) in the *SOLI*<sup>OE</sup> mutant (CaP217,  $P_{TET}SOLI-TAP$ ) after 6 h  
1254 induction in presence of Atc (3  $\mu$ g/ml) in comparison to the uninduced culture (-Atc) or *SOLI*  
1255 expression from its native promoter (CaPJ216, *SOLI-TAP*);  $N=2$ . PSTAIRE was used as a  
1256 loading control. UT, untagged control (SN148). (E) Flow cytometric analysis of cell cycle  
1257 progression in CaPJ215 at indicated time intervals under various growth conditions, as indicated;  
1258  $N=3$ . Dox: 50  $\mu$ g/ml, Met: 5 mM, Cys: 5 mM. (F) *Left*, Hoechst staining of CaPJ215 after 6 h of  
1259 growth under indicated conditions of Dox (50  $\mu$ g/ml), Met (5 mM) and Cys (5 mM);  $n \geq 100$  cells.  
1260 BF bright-field. Scale bar, 5  $\mu$ m. *Right*, percent distribution of the indicated cell phenotypes;  $n$   
1261  $\geq 100$  cells. (G) *Left*, co-localization analysis of Tem1-GFP and Tub4-mCherry in large-budded  
1262 cells of CaPJ218 (*CSA6*<sup>PSD</sup>) under permissive (YPDU-Met-Cys) or repressive conditions (YPDU  
1263 + 5 mM Met and 5 mM Cys). Scale bar, 3  $\mu$ m. *Right*, the proportion of the large-budded cells  
1264 with indicated Tem1 phenotypes;  $n \geq 100$  cells.



1276

1277

**Fig. 7. Ectopic expression and functional conservation of CdCsa6 in *C. albicans*.** (A) Pair-wise alignment of amino acid sequences of Csa6 proteins in *C. albicans* (CaCsa6) and *C. dubliniensis* (CdCsa6) by Clustal Omega, visualized using Jalview. (B) Ectopic expression of CdCsa6 in *C. albicans* by random genomic integration of the ARS-containing plasmid. Vector map of pCdCsa6-GFP-ARS2 depicts the cloned sites of CaURA3, CaARS2 and CdCSA6-GFP. The CdCSA6-GFP fragment contains the GFP tag, CdCSA6 (ORF Cd36\_16290) without the stop codon and the promoter region of CdCSA6. (C) CdCsa6 localizes to the SPB. Representative micrographs showing CdCsa6GFP localization at different cell cycle stages in CaPJ300. Tub4mCherry was used as an SPB marker. Scale bar, 3  $\mu$ m. (D) CdCsa6 functionally complements CaCsa6. Strains with indicated genotypes, (1) SN148, (2) CaPJ300, (3) CaPJ301 and (4) CaPJ302, were streaked on agar plates with permissive (YPDU-Met-Cys) or repressive (YPDU + 5 mM Met and 5 mM Cys) media and incubated at 30°C for two days.

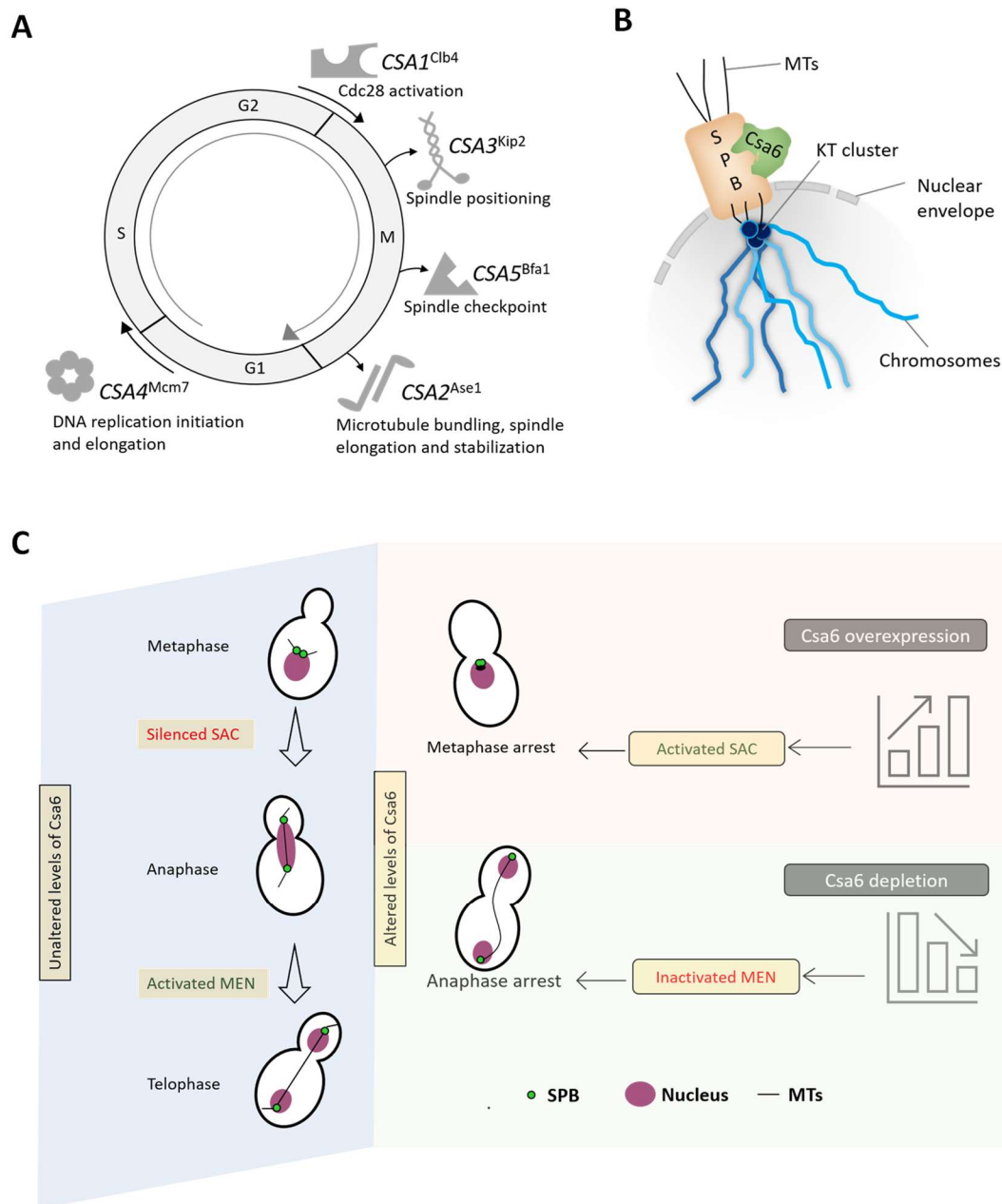
1290

1291

1292

1293

1294

1296  
1297

1298 **Fig. 8. *Csa6* levels are fine-tuned at various stages of the cell cycle to ensure both mitotic**  
 1299 **progression and mitotic exit in *C. albicans*.** (A) A diagram illustrating the functions of the  
 1300 identified *CSA* genes except *CSA6* in various phases and phase transitions of the cell cycle. (B)  
 1301 Schematic depicting the approximate position of *Csa6* with respect to SPB and KT. In *C.*  
 1302 *albicans*, SPBs and clustered KTs remain in close proximity throughout the cell cycle, while *Csa6*  
 1303 remains constitutively localized to the SPBs. (C) A model summarizing the effects of  
 1304 overexpression or depletion of *Csa6* in *C. albicans*. A wild-type cell with unperturbed *Csa6* levels  
 1305 progresses through the mitotic cell cycle. Overexpression of *CSA6* alters the mitotic spindle

1306 dynamics which might lead to improper KT-MT attachments, prompting SAC activation and  
1307 G2/M arrest. In contrast, decreased levels of Csa6 inhibit the MEN signaling pathway, probably  
1308 by affecting Tem1 recruitment to the SPBs, resulting in cell cycle arrest at the anaphase stage.

1309

1310

1311

1312

1313

1314

1315

1316

1317

1318

1319

1320

1321

1322

1323

1324

1325

1326

1327

1328

1329

1330

1331

1332 **Table 1. Overexpression phenotypes of CSA genes in *C. albicans* and *S. cerevisiae***

1333

| <b>CSA gene</b> | <b><i>C. albicans</i> ORF no.</b> | <b><i>S. cerevisiae</i> homolog</b> | <b>Overexpression phenotype (<i>C. albicans</i>)</b>    | <b>Overexpression phenotype (<i>S. cerevisiae</i>)</b>   | <b>Reference</b> |
|-----------------|-----------------------------------|-------------------------------------|---|--|------------------|
| <i>CSA1</i>     | 19.7186                           | <i>CLB4</i>                         | Increased CIN involving non-CL events                   | Shift towards 2N (diploid) DNA content   | 100              |
| <i>CSA2</i>     | 19.7377                           | <i>ASE1</i>                         | Increased CIN involving non-CL events                   | i) CIN involving loss of an artificial chromosome fragment or rearrangements/ gene conversion events.<br>ii) Spindle checkpoint dependent delay in entering anaphase upon HU treatment | 14, 75           |
| <i>CSA3</i>     | 19.1747                           | <i>KIP2</i>                         | Increased CIN involving non-CL events                   | Shift towards 2N (diploid) DNA content   | 81, 100          |
| <i>CSA4</i>     | 19.202                            | <i>MCM7</i>                         | Shift towards 4N (diploid) DNA content, G2/M arrest     | NA   | NA               |
| <i>CSA5</i>     | 19.608                            | <i>BFA1</i>                         | Shift towards 4N (diploid) DNA content, anaphase arrest | Shift towards 2N (diploid) DNA content, Anaphase arrest  | 101              |
| <i>CSA6</i>     | 19.1447                           | NA                                  | Shift towards 4N (diploid) DNA content, G2/M arrest     | NA   | NA               |

1334 NA, not available

1335

1336

1337

1338

1339

1340

1341

1342

1343

## Supplementary Files

This is a list of supplementary files associated with this preprint. Click to download.

- [Dataset1.xlsx](#)
- [Jaitlyetal.supplenaturecom.pdf](#)